Bench-Scale Characterization of Joints and Coatings

Akhilesh Kulkarni

Thesis submitted to the faculty of the Virginia Polytechnic Institute and State University
in partial fulfillment of the requirements for the degree of

Master of Science
In
Mechanical Engineering

Brian Y. Lattimer, Co-Chair
Scott W. Case, Co-Chair
Scott Huxtable

May 18, 2023
Blacksburg VA

Keywords: ASTM E119, Fire resistance test, thermo-structural test, scaling laws, intumescent coating, half-lap joint

Bench-Scale Characterization of Joints and Coatings

Akhilesh Kulkarni

ABSTRACT

The ASTM E119 is a large-scale test used to qualify assemblies for fire resistance, including heat transmission and structural integrity. The test requires specialized furnaces and full-scale assemblies that are 3.0 m (10 ft) or more on each side, making it very expensive to perform. In this study, we investigated the feasibility of the scaling methodology for a reduced-scale fire resistance test on different types of wood-based structures, specifically commercially available intumescent coating applied onto wood and bolted lap joints in wood. We build upon a previously developed scaling methodology for wood and gypsum boards, which integrated geometric scaling, Fourier number time scaling, and furnace boundary condition matching. Intumescent coating presents a particular challenge in scaling in that it expands when exposed to fire conditions. To account for this expansion, we identified a relationship between initial dry film thickness and final expanded thickness through cone calorimeter tests and integrated it into a modified scaling methodology. This approach was then validated through fire exposure tests in furnace on wood samples painted with intumescent coating at full, half, and quarter scales. Finally, we demonstrated the scaling laws for joints under combined thermo-structural loading, by subjecting wood-based half-lap joint samples to combined bending and thermal loading at half and quarter scale. The samples were subjected to static three-point bending with the load scaled to achieve structural similitude, while simultaneously being exposed to a scaled fire exposure on the bottom surface. Our study provides insights into the practical application of scaling methodology for testing the fire resistance of joints and fire-resistant coated wood, paving the way for more cost-effective and quicker fire testing for the wood-based composite industry.

Bench-Scale Characterization of Joints and Coatings

Akhilesh Kulkarni

GENERAL AUDIENCE ABSTRACT

The ASTM E119 is a critical test standard that evaluates the fire resistance of various building materials, including wood-based structures. However, the standard tests are quite expensive due to the need for specialized equipment and large-scale samples. In this study, we explored the potential of using a scaled-down fire resistance test on different types of wood-based materials, including commercially available fire-resistant coated wood and joints.

We built on existing scaling methods for wood and gypsum boards and adapted it to account for the unique properties of intumescent coating - a fire-resistant material that expands when exposed to high temperatures. By conducting a series of tests, we developed a modified scaling approach to accommodate the expansion of the coating.

We then validated this new method by performing fire exposure tests at various scales on wood samples coated with intumescent coating. Finally, we adapted the scaling methods to account for wood based bolted joints. We tested the fire resistance of wood-based half-lap joints under combined heat and structural stress at smaller scales.

Our study offers valuable insights into a more cost-effective and efficient method for testing fire resistance in wood-based structures. By providing a reliable scaling approach for fire-resistant coated wood and joints, our work has the potential to make fire testing more accessible for the wood composite industry, ultimately leading to safer and better-performing buildings.

Acknowledgements

I would like to express my profound gratitude to the Wood Based Composites Center, a National Science Foundation Industry/University Cooperative Research Center (Award number - 1624536), for their generous financial support of my research, which made this research possible.

I am deeply thankful to my advisors, Dr. Brian Lattimer and Dr. Scott Case, for providing me with this research opportunity and for their invaluable guidance throughout my thesis work. Their continuous support, constructive feedback, and active involvement in the experimental tests have been instrumental in the successful completion of my thesis.

I would also like to express my appreciation to Dr. Scott Huxtable, my third advisory committee member, for his valuable contributions and insights.

My heartfelt thanks go to my lab mates, Michael Gangi, who assisted me in conducting the furnace tests and provided guidance in modifying the test fixtures, as well as Steven Wong, Mehrnoush Farhadi, Rezawana Islam, Mehran Islam, and Aysenur Ates, who contributed to a positive and collaborative work environment, making my time in the lab both enjoyable and productive.

I am grateful to my friends at Virginia Tech for making my experience in Blacksburg enriching and memorable. Above all, I am profoundly grateful to my parents Archana and Pravin Kulkarni for their constant support and encouragement from India throughout this journey. Their love and steadfast belief in me made this accomplishment possible.

Table of Contents

List of Figures

List of Tables

Nomenclature

b width [m]

cp specific heat capacity [J/kg-K]

d thickness [m]

Fo Fourier number

h_c convective heat transfer coefficient [W/m^2 -K]

I_y moment of inertia [m^4]

k thermal conductivity [W/m-K]

L length [m]

L_c Characteristic length [m]

P force [N]

T temperature [K]

t time [s]

Greek

α thermal diffusivity [m^2 /s]

δ deflection [m]

ϵ emissivity

ρ density [kg/m^3]

σ bending stress [Pa]

τ_{xy} shear stress [Pa]

χ scaling factor

Subscripts

1 full-scale

2 reduced-scale

max maximum

Chapter 1 Introduction

Establishing a structure's safety during a fire is vital, and fire-resistance testing is commonly employed to analyze a structure's reaction to fire. Fire-resistance testing examines an assembly's capacity to hinder fire propagation and structural failure by evaluating the transmission of heat and hot gases through the assembly. Due to the complex nature of materials' behavior in fire conditions, numerous building products necessitate testing under combined thermo-structural loads.

A full-scale fire resistance test is the conventional method for assessing the fire endurance of structures. Test specimens must accurately represent field construction, necessitating that all dimensions and details be constructed as if they were being installed in a building. As a result, large-scale fire resistance tests are costly and challenging to conduct, leading to a limited amount of test data.

ASTM E119 [1] is a standard for large-scale tests employed to evaluate assemblies for fire resistance, including heat transmission and structural stability. For ASTM E119, typical test specimens for floor and wall assemblies must be at least 3.0 m (10 ft.) or more on each side. The test, though useful in capturing the various failures observed in large scale test specimens, has its limitations in a practical aspect. The standard method requires specialized furnaces and full-scale assemblies, making it very expensive and time consuming to perform.

1.1 Motivation

Owing to the costly nature of large-scale tests, devising a more affordable, smaller-scale test capable of determining the worthiness of investment in a new product during the early stages of product development would be advantageous, saving the testers valuable time and money by avoiding a large-scale thermo-structural test for every prototype. A previous study accomplished this by creating a bench-scaling methodology that scaled down the ASTM E119 furnace exposure, thereby reducing the test and sample size while preserving the thermo-structural similitude with the original large-scale test Ref. [2]. It focused on using dimensional lumber and plywood boards as the test samples. However, there are many wood-based structures, like wood joints and fire-resistant material coated wood substrates which are not directly covered by this scaling methodology. Because structures containing these features also require a similar qualification by

the ASTM E119 test, it would be beneficial in terms of time and money if the scaling methodology were extended to other wood-based structures. This is the central motivation of this research.

1.2 Previous Work on Intumescent Coatings

Intumescent coatings (ICs) are an essential passive fire protection measure for steel and wooden structures. These coatings consist of a complex formulation that, when exposed to high temperatures, expands, and forms an insulating char layer, reducing the heat transfer to the underlying substrate and delaying structural failure. The performance of ICs depends on various factors such as their formulation, the heating conditions, and the substrate material. This literature review aims to provide an overview of the existing research on intumescent coatings, focusing on their formulations, numerical models, experimental techniques, and instrumentation.

1.2.1 Types of intumescent coatings

The two types of intumescent coatings are silicate and organic. There is a distinction between them based on the range of applications and it is important to identify which type would be appropriate for our study.

Intumescent silicate coatings are primarily used for fire protection of wood, as they demonstrate poor water resistance. Several studies have explored different formulations for this type of intumescent coatings. Puri-Khanna reported a fire-retardant, intumescent, ceramic coating for structural steel and wood, which was prepared by mixing a finely ground borate compound with sodium silicate solution, then drying, pulverizing, and adding it to a second sodium silicate solution [3]. Another intumescent aqueous composition contained alkali silicate, clay, and inorganic materials like hydrated aluminum oxide, hydrated borate, carbonates, and bicarbonates. This formulation could be applied to metal, wooden, and polymeric materials, providing a thermal barrier when exposed to high temperatures.

Puri-Khanna also reported an intumescent composition containing sodium silicate, cenospheres, water, and sodium tetradecyl sulfate, which was used for wood structural panels to offer protection against high temperatures and prolonged heat exposure. This study also found that an aqueous fire

barrier composition could be prepared using a polymer latex and an intumescent agent that included granular alkali metal silicate.

Organic intumescent coatings have been widely researched due to their versatile applications. Hassan et al. studied a butyl acrylate polymer with a mixture of melamine phosphate and pentaerythritol, combined with polyurethane (PU) coatings [4]. Puri-Khanna formulated an intumescent coating using dicyandiamide phosphate along with pentaerythritol, which was particularly suitable as a clear coat for wood and wood-related surfaces [3]. Lucherini et al. found that compositions based on amino-resins could be successfully applied to wooden substrates [5]. Hussain et al. explored the use of polysiloxane microencapsulation of ammonium polyphosphate (APP) for polyolefins [6].

In summary, intumescent silicate coatings are predominantly used in interior applications and fire stops due to their poor water resistance. Organic intumescent coatings, on the other hand, offer a broader range of applications, including fire protection for wood, structural steel, and glass fiber-reinforced polyester (GRP) composites.

1.2.2 Numerical models of coating behavior

Numerical models have been widely utilized to study the behavior of intumescent coatings (IC) under various test conditions.

Staggs et al. investigated the behavior of an experimental intumescent coating under various test conditions. They developed a model guided by experimental observations and analytical data to better understand the IC's performance [7]. Zhang et al. [8] developed a mathematical model to simulate the expansion process and global behavior of intumescent coatings. Although their model predictions were in good agreement with cone calorimeter and furnace fire test results, it was based on many assumptions that did not reflect the physical and chemical behavior of ICs, such as the loss of produced gases to the environment.

Chang et al. [9]and Asaro et al. [10] both employed inverse estimation methods based on the steel substrate, which provided accurate and relevant results in their respective models. Kandare et al.

[11] applied the same intumescent coating as Asaro on fiber-polymer laminates, extending the research to a different substrate material.

Cirpici et al. [12] introduced a multi-layer model capable of predicting the IC behavior and effective thermal conductivity under different dry film thicknesses (DFT), steel section factors, and fire conditions.

The simplified models, such as those proposed by Staggs, Zhang, Cirpici, Chang, and Asaro, were mainly based on experimental investigations of intumescent painted thin steel sheets exposed to uniform heating conditions. However, the expanded intumescent foam is a highly heterogeneous material consisting of a solid matrix, pores filled with air, and thermal degradation gases. Therefore, the heat transfer process involves conduction, convection, and radiation, along with additional heat production or sink due to exothermic and endothermic chemical reactions.

Despite the level of sophistication in these models, they still face limitations in accurately predicting fire protection provided by intumescent systems in real-life fire scenarios. Some of the limitations include:

- Difficulties in determining dynamic, thermophysical, and kinetic chemical parameters of the paint, as they are challenging to measure in standard small-scale research apparatus such as Thermo-Gravimetric Analysis (TGA) and Differential Scanning Calorimeter (DSC).
- Challenges in determining the effects of cracking, delamination, and erosion of the expanded coating due to turbulent combustion gases, which are typically observed in large-scale furnace tests and real-life fire scenarios.
- Issues related to the effects of the steel member's cross-section shape (section factor), which influences coating cracking, reduces insulation efficiency, and requires the inclusion of mechanical-stress and rheological effect sub models.

Despite these limitations, the numerical models presented in the literature have provided valuable insights into the behavior and performance of intumescent coatings under various conditions. [13]

1.2.3. Experimental characterization of coatings

1.2.3.1 Initiation of coating expansion

In one study [14] the onset of expansion in intumescent coatings was investigated based on their initial applied dry film thickness (DFT). Three DFT categories were examined: Low DFT (0.89-1.20 mm), Medium DFT (1.54-2.01 mm), and High DFT (2.71-3.04 mm). The expansion behavior was observed as a function of steel temperatures and average coating temperatures. For Low DFT samples, swelling initiated when steel temperatures were between 170 and 260 °C and average coating temperatures ranged from 360 to 510 °C. Medium DFT samples exhibited expansion initiation at steel temperatures between 100 and 260 °C and average coating temperatures from 350 to 500 °C. Lastly, in the case of High DFT samples, expansion began at steel temperatures between 90 and 200 °C, and average coating temperatures were within the range of 370 to 480 °C. Thus, the initiation of expansion in thin intumescent coatings is affected by the initial applied dry film thickness.

1.2.3.2 Expansion ratio

One study [5] examined the expansion behavior of timber samples coated with different dry film thickness (DFT) layers: thin (0.5 mm DFT), medium (1.3 mm DFT), and thick (2.1 mm DFT). The objective was to observe the relationship between the initial DFT and the resultant char thickness upon expansion. The findings revealed that timber samples with thin, medium, and thick coating layers expanded up to char thicknesses of approximately 19 mm, 22 mm, and 35 mm, respectively, highlighting the impact of the initial coating thickness on the expansion development during exposure. Thus, the maximum thickness that each coating layer can achieve is limited by the initial applied thickness of IC. This means that the expansion ratios depend on the initial DFT.

The initial applied DFT of IC controls the rate of temperature increment within coated timber samples. A thicker layer of intumescent coating had a higher delaying effect on the onset of charring due to the significant expansion process and the thicker developed char [14].

1.2.3.3 Heating conditions and testing setups

Numerous studies have demonstrated that diverse heating conditions can result in distinct char structures, expansion ratios, and overall expansion processes. Generally, intumescent coatings

exposed to rapidly developing fires tend to undergo a more comprehensive reaction, leading to optimal expansions [15]. Specifically, Han et al.'s [16] study revealed that the full development of the intumescent coating was achieved at incident radiant heat fluxes exceeding 35 kW/m^2, while Lucherini et al. [14] found that the minimum incident heat flux required to initiate expansion was above 23 kW/m^2. Conversely, intumescent coatings subjected to slowly progressing fires may fail to completely react, resulting in suboptimal expansion and performance [17]. In some experimental tests, low heating regimes even caused melting, delamination of the coating, or char cracking accompanied by incomplete expansion [18] [19].

Therefore, the rate of intumescent coating expansion is influenced by the heating conditions.
The furnace is a widely used method for evaluating the performance of intumescent coatings by employing the standard fire curve. In numerous research studies, the standard fire curve serves as the primary heating condition applied to unloaded protected samples, with the evolution of protected steel temperatures being the sole performance control parameter. Recently, some researchers have started incorporating various non-standard temperature-time fire curves in furnace testing.

Owing to the expensive and time-consuming nature of standard furnace testing, researchers have devised bench-scale and laboratory-scale experiments to examine intumescent coating behavior under different fire conditions. One common method involves exposing coated steel samples to constant radiant heat fluxes using a cone calorimeter [20]. However, this technique has several limitations, including the impact of the distance between the sample and the cone heater's bottom on results, non-uniform incident heat fluxes, and uncertainties regarding the net heat flux absorbed by the test sample during the expansion process [21] [22], [23].

Elliott et al. [18] suggested the H-TRIS method to investigate the performance of reactive coatings exposed to varying time-histories of incident radiant heat flux. This fire test method controls the thermal boundary conditions imposed on a test sample by maneuvering an array of high-performance radiant panels. The approach offers considerable advantages over traditional testing in terms of reliability, repeatability, versatility, speed, and cost, and allows for the visual inspection of test samples during fire testing [5].

Despite these advances, the research community has not yet agreed on a universal testing methodology for intumescent coatings.

1.2.3.4 Thermal conductivity

Thermal conductivity is a critical parameter in assessing the insulation and performance of intumescent coatings. Lucherini et al. compiled three definitions in the literature [13]:

- Effective thermal conductivity: This concept evaluates the coating thermal conductivity considering the initial dry film thickness. Although widely adopted in engineering design practice, it provides an imprecise description of the thermal behavior of the protective layer.
- Effective constant thermal conductivity: This is the temperature-averaged value of the temperature-dependent effective thermal conductivity within the temperature range of interest for fire resistance design of steel structures, usually 400-600°C.
- Apparent thermal conductivity: This is evaluated considering the actual swelled coating thickness and relies on measurements of the in-depth temperatures within the swelled coating. Inverse heat transfer models are usually implemented to calculate the apparent thermal conductivity of intumescent coatings.

While the first two definitions simplify the design process, they do not clearly represent the effectiveness of intumescent coatings. In contrast, the apparent thermal conductivity enables explicit calculation of the transient temperature gradients within swelled intumescent coatings using simple heat transfer finite-element models. However, this methodology has been adopted in only a few research studies due to experimental difficulties related to obtaining accurate measurements of the in-depth temperature distributions without disturbing the expansion process. The third definition has been modified in a few papers, such as those by Asaro et al. [10] and Chang et al. [9], to estimate the thermal conductivity using surface temperatures and mass loss rate histories from the experimental measurements. These modified approaches help in understanding the thermal behavior of intumescent coatings and can be potentially useful for predicting their performance under various fire conditions. Various experimental methods, including the Hot Disk Thermal Constants Analyzer, Laser Flash Analysis (LFA), and X-ray computed tomography, have been employed by researchers to determine thermal conductivity of intumescent coatings ([7] [13]

[24] [25]). However, our scaling approach requires only temperature measurements to investigate thermal similitude. Therefore, we will not measure thermal conductivity in our study.

In summary, experimental results show that the performance of intumescent coatings is influenced by factors such as dry film thickness, heating conditions, and thermal conductivity. Various experimental techniques, such as furnace testing, cone calorimetry, and H-TRIS, have been developed to evaluate the behavior of intumescent coatings under different fire conditions. However, the research community has not yet agreed on a universal testing methodology for intumescent coatings. While some definitions of thermal conductivity simplify the design process, they may not accurately represent the effectiveness of intumescent coatings. Further research is needed to improve the accuracy and reliability of these experimental techniques and better understand the behavior of intumescent coatings in real-life fire scenarios.

1.2.4 Characterization of coating properties

The investigation of intumescent coatings (IC) properties typically requires a comprehensive analysis of various factors, including temperature, initial and final coating thickness, optical properties, and coating degradation kinetics.

1.2.4.1 Temperature measurements

Accurate temperature measurements are crucial in intumescent coating studies. Researchers ([26], [27]) usually measure temperature at several points, such as the exposed surface, intumescent/laminate interface, mid-thickness of the laminate, and the unexposed laminate surface, primarily using thermocouples. Alternative techniques include thermographic phosphors for measuring intumescent coating surface temperature [26], infrared pyrometers for surface temperature measurement [27], and temperature sensors placed within the expanding intumescent char for calculating thermal conductivity [28]. To obtain precise temperature readings within wood samples, researchers suggest positioning in-depth thermocouples perpendicular to the primary heat transfer direction inside the timber sample [29]. However, placing sensors within the expanding coating to measure temperature disturbs the expansion process.

1.2.4.2 Initial and final coating thickness measurements

Standard methods and equipment for applying intumescent coatings on various substrates are consistently used across studies, and digital thickness gauges measure the dry film thickness (DFT) ([6] [19] [30]). The drying period depends on the IC type and substrate, though specific drying times are often not mentioned ([5], [19] [31]). Researchers employ techniques like digital cameras, MATLAB image processing, Digital Image Correlation (DIC), and real-time image processing of videos to measure intumescent coating expansion ([11] [19] [30] [31]). Among these, MATLAB image processing offers simplicity and high accuracy, while real-time image processing of videos and DIC are more complex but accurate. However, in our study there is no need to control the test inputs like heating rates with respect to the real-time expansion observed. Therefore, image processing in MATLAB would be the best method to capture expansion because of its simplicity.

1.2.4.3 Optical properties

Optical properties, such as emissivity, absorptivity, and reflectivity, significantly impact test sample heating conditions. Lucherini et al. analyzed these properties using an Integrating Sphere System (ISS) apparatus combined with Fourier-Transform Infrared Spectroscopy [19].

1.2.4.4 Coating degradation kinetics

Thermo-Gravimetric Analysis (TGA) is a primary testing methodology for understanding the degradation processes of thin intumescent coatings and engineering effective formulations. In the studies reviewed, researchers conducted TGA tests using different instruments and heating rates [7]. TGA results have shown that oxygen concentration influences degradation kinetics, with mass loss generally occurring more slowly in air than in nitrogen. However, TGA testing involves small samples and relatively low heating rates, which marginalizes the influence of heat transfer.

From the literature study, we conclude that

1. Most of the prior research on intumescent coatings was conducted using steel as a substrate rather than wood. There are various factors like charring, crackling, etc. which affect wood that are not relevant to coating-steel assemblies. More research is needed to study these effects.
2. Numerical models have considered many assumptions to simplify the complex coating expansion process. Those numerical models typically assumed a constant expansion ratio.

However, in a recent experimental study, the expansion ratio has been found to have been dependent on various factors such as the initial coating thickness, heating rate, etc.

3. For scaling purposes, prior models assuming a constant expansion ratio will not work. In furnace testing, the heating rates will be different for different scales leading to different expansion ratios. Developing and implementing a computational model incorporating this behavior would be a significant effort in itself. Thus, our focus is limited to experimental study to scale the intumescent coating.
4. We have identified one study previously conducted varying the dry film thicknesses in intumescent coatings to study the effect on final expanded coating thickness. However, no relation was developed between the two. Thus, there is a need to study the expansion process in detail and to develop a methodology which would relate the initial dry film thickness to its final expanded thickness and then test this developed relation for accuracy.
5. We need to show thermal similitude across different scales which requires temperature gradient comparison. Therefore, we would need temperature measurements from the experiments. Thermocouples have been used to measure substrate temperatures along the depths. It has been noted that thermocouples should be placed orthogonal to primary direction of heat transfer for accurate measurements.
6. Coating expansion has been successfully measured using Digital Image Correlation and image processing in past studies. Image processing is relatively simpler of the two and is accurate enough to implement in our tests for developing a coating expansion relationship. There is a possibility to measure real-time expansion of coating as well. However, there is no need to control the test inputs with respect to the real-time expansion observed in our study.

1.2 Previous work on Joints

Wood-based joints are primarily wood boards with steel fasteners in most cases. Thus, there is a good possibility that they would behave similar to how wood boards behave under exposure to fire. Charring for instance, could have a big impact on scaling joints as well. As the nature of scaling might be similar, we looked at past studies which presented methodologies for scaling fire resistance in wood. Gangi et al. [2] presented methodology for scaling thermal and structural response in wood. This study will use a similar methodology to scale wood joints to maintain

thermal and structural response. However, instead of keeping length and width same across different scales, we will use and modify this methodology with a linear scaling in all geometric parameters on the joint.

However, as the wood joints are to be bolted, it was also necessary to study the effect of bolts on the thermo-structural scaling.

1.3.1 Impact of bolt diameter

Maraveas et al. [32] conducted a comprehensive analysis of the behavior of timber connections in recent years. Prior research has largely focused on wood-wood-wood (WWW), wood-steel-wood (WSW), and steel-wood-steel (SWS) joint types, with most investigations centered on the influence of load variation on fire resistance [33], [34] [35]. A few studies have explored the impact of fasteners on fire resistance in the context of bolts and dowels [35], [36]. However, additional experimental research is needed to better understand the effect of fastener type. The previously gathered experimental data encompasses connections featuring bolts, dowels, and screws, although differing load ratios were employed. One study [34] found that joints using screws exhibited higher fire resistance (approximately 10 minutes) than those employing bolts, given the same load ratio. The same author attributed this difference to the increased heat transfer to the timber caused by the bolt head, which likely contributed to the diminished fire resistance observed in the tested bolted connections. While fasteners with varying diameters were used in the tested connections, a direct comparison is only feasible in the experiments carried out by Dhima [36]. Joints using 12 mm bolts displayed similar fire resistance to those with 20 mm bolts, despite differing load ratios (33% and 12% respectively). Although this suggests that larger fasteners may offer better fire resistance, it is important to consider that the number and arrangement of fasteners were not identical. Further tests should be conducted with consistent load ratios and connector layouts to confirm these findings.

1.3.2 Influence of edge distance

At room temperature, current standards [37] [38] account for net tension failure in wood-wood-wood connections by establishing minimum edge distance requirements based on the type of connector used. A 1.5d edge distance, with d being the fastener diameter, is specified in the

Canadian Standard CAN/CSA-O86-09 [39]. However, the appropriateness of these edge distances must be reconsidered under the effects of elevated temperatures, as the reduction of cross-section due to charring may impact their effectiveness. Experimental data addressing this issue is limited. Noren [40] investigated the effect of the edge distance in nailed WWW joints, reporting that charring parallel to the side members resulted in a more rapid decline in load-bearing capacity for edge nails, causing them to fail differently than those located in the middle. Laplanche [35] found that increasing the material towards the edge by 43% resulted in a 60% and 30% increase in fire resistance for load ratios of 10% and 30% respectively. To prevent premature failure, Peng et al. [41] proposed increasing edge distances by the product of the charring rate and the desired fire resistance.

Based on the provided literature review, there are several gaps in the current understanding of wood-based joints, specifically related to the effects of fastener type, fastener diameter, and edge distance under fire conditions:

- Fastener Type: While a few studies have compared the fire resistance of joints using bolts and dowels, additional experimental research is needed to better understand the impact of different fastener types on the fire resistance of wood joints.

- Bolt Diameter: Although connections with 12 mm and 20 mm bolts have been compared, the load ratios and fastener arrangements were not consistent across the experiments. Further testing should be conducted with the same load ratios and joint layouts to determine if larger fasteners indeed provide better fire resistance.

- Edge Distance: The impact of edge distance on the fire resistance of wood joints remains underexplored, especially under elevated temperature conditions. Existing standards may need to be reevaluated to account for the effects of charring on cross-sectional reduction. More experimental data is needed to address this gap in knowledge and inform potential revisions to edge distance requirements.

Addressing these gaps in the literature would contribute to a more comprehensive understanding of the performance of timber connections under fire conditions, ultimately leading to improved design and safety standards for structures employing these connections.

1.3 Research Objectives

The main aim of this research is to extend the thermo-structural scaling methodology and investigate its feasibility to cover different types of wood-based structural assemblies. Specifically, the focus is on scaling commercially available fire-resistant coated wood, and wood joints among the different wood-based structural assemblies.

This aim has been expanded into the following objectives:

1. Scaling of coatings
    - 1.1 Evaluate how to scale commercial coatings and assess the scaling performance on wood
    - 1.2 Extent to which coatings can be scaled
2. Scaling of joints
    - 2.1 Evaluate the performance of scaled joint assemblies
        - 2.1.1 Evaluate feasibility of scaling joints through a series of bench-scale furnace tests

Based on these objectives, this study should be able to recommend an approach to evaluate fire-resistant coatings and joints.

Chapter 2 Coatings

First, we look at the differentiation between flame spread and fire resistance, both of which are characteristics of coatings. Flame spread is determined by the distance that a flame travels along a material in a limited time and is evaluated using the ASTM E84 standard test. According to this standard, materials are classified into three classes: A, B, and C. Inorganic cement board is rated 0 and red oak flooring is rated 100 which are arbitrarily assigned. A is from 0-25, B is from 26-75 and C is from 76-100. On the other hand, fire resistance considers limited heat transmission through the assembly, preventing flame passage or hot gas ignition of cotton waste and maintaining structural integrity. Fire resistance is measured using the ASTM E119 test, wherein a material sample is exposed to a temperature-controlled fire, and the structural assembly receives an hourly rating (e.g., 1 hr., 2 hr., etc.). Coatings applied to wood are often geared toward one behavior or the other. Acrylics, epoxies, polyurethanes, chlorine based, phosphorous based, bromine based, etc. are all classified as flame retardants. They are usually characterized by flame spread. Other types of coatings such as intumescent coatings or MgO based coatings are characterized by fire resistance.

Since we wanted to scale ASTM E119 test which examines fire resistance of an assembly, we focused on coatings characterized by fire resistance. Because of project time constraints, we could only investigate one coating type. Thus, our primary focus in this chapter is on intumescent coatings (ICs), a type of fire-resistant coating that expands when exposed to fire conditions, forming a low thermally conductive layer that protects the substrate.

ICs are passive fire protection systems, comprising three main fire-retardant additives: an acid source (e.g., ammonium polyphosphate, APP), a blowing agent (e.g., melamine, MEL), and a carbon source (e.g., pentaerythritol, PER). These additives provide a range of properties, including generating acid compounds in situ, producing gases when heated, and forming an insulating char layer that maintains structural integrity.

However, when applied to wood substrates, ICs may face certain challenges, such as losing their performance as fire retardant chemicals, leaching from the wood surface, and being affected by

hygroscopic properties of fire-retardant additives. These issues limit their usage in exterior wood sidings and indoor spaces with high relative humidity levels. In this chapter, we will investigate the scaling methodology for fire resistance testing on wood-based structures coated with ICs.

We investigated commercially available ICs for both steel and wood substrates. For steel, we examined Firetex® FX5120, Albi Clad TF, and Thermo-Sorb® 263, all of which are thin-film and tested for fire resistance according to ASTM E-119. For wood, we studied Albi Clad FP and FlameOFF® Fire Barrier Paint, both of which are thin-film, water-based, and tested for fire resistance following the ASTM E119/UL 263 standards. Based on the availability we selected FlameOFF® Fire Barrier Paint.

2.1 Scaling Approach

In the previous study of Gangi et al. [2], a thermo-structural scaling methodology was developed combining uniform geometric scaling, Fourier number time scaling, and boundary condition matching. The uniform geometric scaling meant that when an object underwent uniform scaling, it became a smaller version of the original, with similar geometric characteristics. The degree of scaling was determined by the uniform scaling factor, denoted by χ, which represented the ratio of the reduced-size dimensions to the full-size dimensions. For example, a ¼ scale test corresponded to χ = 0.25. Figure 2.1 illustrated the original assembly, which had width a, length b, and thickness d. To preserve structural similarity, the scaled assembly had to have dimensions that were proportional to those of the original, when subjected to the same load per unit area p.

$$a_{scale} = \chi a_{orig} \tag{2.1}$$

$$b_{scale} = \chi b_{orig} \tag{2.2}$$

$$d_{scale} = \chi d_{orig} \tag{2.3}$$

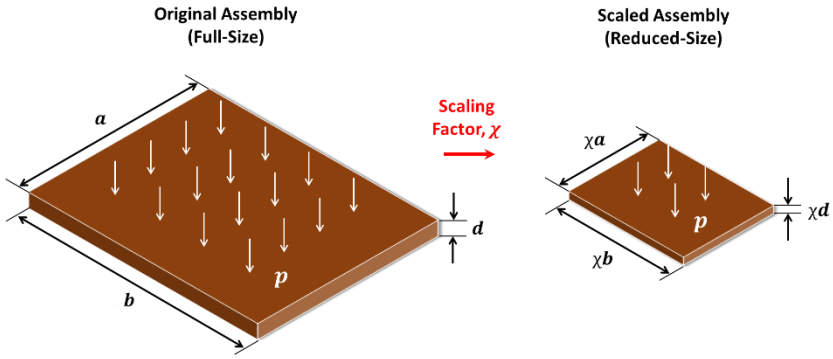

Figure 2.1 Comparison of dimensions from original to scaled test from literature [2]

Fourier number time scaling meant that for there to be thermal similarity at two scales the time scaled as follows:

$$Fo = \frac{\alpha\tau_{orig}}{d^2} = \frac{\alpha\tau_{scale}}{(\chi d)^2} \Rightarrow \tau_{scale} = \chi^2\tau_{orig} \quad (2.4)$$

The characteristic time for the scaled test differed by a factor of χ^2 compared to the original test. This meant that for a ¼ scale test with χ = 0.25, time scaled as 0.0625. As a result, a ¼ scale test with 225 seconds of fire exposure was the full-scale equivalent test time of 3600 seconds.

Boundary condition matching was also calculated in Ref. [2] for ½ and ¼ scales as shown in Figure 2.2. This figure shows that in order to achieve the same surface temperature as a function of effective time at smaller size scales, the magnitudes of the temperature in the standard ASTM E119 fire curve had to be increased.

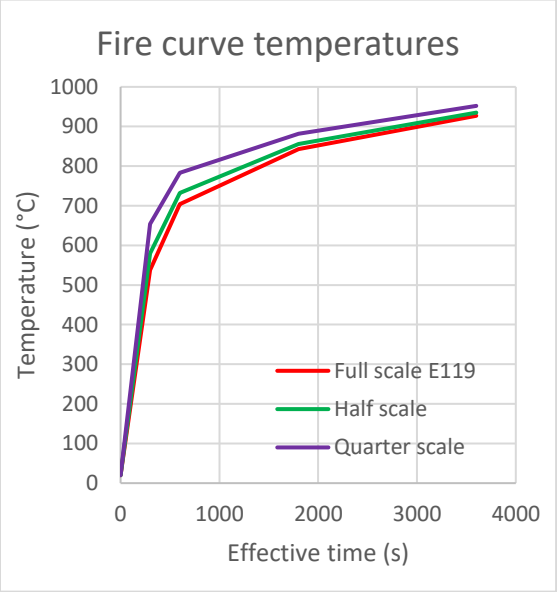

Figure 2.2 Modified scaled furnace time-temperature at different scales from literature [2]

This previous scaling study was conducted on uncoated wood samples. We wanted to extend this scaling to wood samples with a fire protection coating on the exposed surface. The Fourier time number scaling which was applied to wood substrate thickness above is expected to also apply to coatings if the thickness can be scaled. Similar to the wood part of the sample, the time scaling will go as χ^2 and the coating thickness should scale as χ to maintain the heat transfer similitude through the thickness, as shown in Figure 2.3.

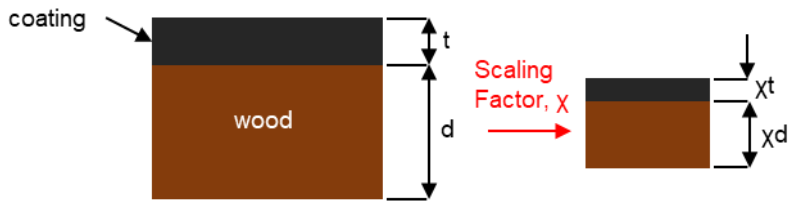

Figure 2.3 Scaling in coating-wood substrate structural assembly

While this approach should be suitable for non-reactive commercial coatings, some coatings, such as intumescent coatings (IC), may require further modifications to complete the methodology. IC is unique among the commercially available fire protection coatings in that it expands when exposed to fire conditions. The scaling factor χ in this case would refer to the final coating thickness after expansion to char. We would assume an instantaneous coating expansion in our scaling approach. Because of this characteristic, we need to identify a specific relationship between the final coating thickness of IC after expansion and its initial dry film thickness (DFT). This would complete the scaling part of our methodology for coatings which expand when exposed to fire conditions.

2.2 Experimental Approach

In the previous section, we outlined an approach to scale both the coating and the wood substrate for the ASTM E119 fire resistance test. We also mentioned the need to find a relationship between the dry film thickness and final expanded coating thickness for the case of intumescent coated wood substrate.

There are two ways to go about getting this relation. One would be modeling the IC expansion to obtain a relationship and other would be experimentally finding the relationship. Many past studies who have modeled the IC exposure to fire have assumed a constant IC expansion ratio to simplify the complex models. A few experimental studies have shown that the expansion ratio is not constant but depends on several parameters, significantly the rate of the heating flux. Also, as seen in the past studies which focused on modeling, there is a gap between what the models predict, and the actual expansion observed in experimental studies. Given the time required for the modeling approach and the uncertainties involved, we determined that although it was more

expensive to perform a test, the experimental approach would effectively save costs with it being conducted more quickly compared to modeling. Thus, it was the best method to establish the IC expansion relationship for our methodology.

Having established the need for an experimental approach to determine the relationship between the DFT and final expanded coating thickness of IC, we needed to choose a suitable testing setup. This was performed in the cone calorimeter apparatus was due to the following advantages:

1. Lower cost
2. Smaller test sample
3. Shorter testing time

Although there was some uncertainty as to whether the relationship established in the cone calorimeter test would be applicable in fire resistance furnace tests, given the differences in heating rates between the two setups and the dependence of IC expansion on heating rate, previous studies have shown this dependence. Nonetheless, considering the advantages offered by the cone calorimeter, we decided to use this test to establish the relationship and later validate it during fire resistance tests conducted in the furnace.

Based on this, these are the objectives of the cone calorimeter tests:

1 Initial assessment of expansion of the intumescent coating (IC) for scaled dry film thicknesses (DFTs) under a constant heat flux

2 Identify the DFTs required for the later small-scale fire resistance furnace tests

With the relationship defined, the scaling part of the methodology was complete for most of the fire-resistant coatings including IC. We identified the dry film thicknesses required for scaling the intumescent coatings. Based on the conclusions derived from scaling approach in Section 2.1 and the relationship of DFT and expansion ratio, we created a test matrix for tests in furnace.

Because of the time constraints in delivering the results to the sponsors of the project, we would not have been able to evaluate the scaling methodology on the various types of fire-resistant coatings commercially available. Because of its expansion when exposed to fire conditions, and as it required an addition to the scaling approach, out of all the coatings, the intumescent coating

was the most challenging. Therefore, we decided to focus our attention on testing the scaling approach on intumescent coating painted wood substrate with the objective of determining the extent to which the intumescent coating can be scaled maintaining the thermal similitude in scaled lumber.

2.2.1 Cone calorimeter testing

The cone calorimeter is widely used in the field of fire safety and is used to evaluate the flammability and fire behavior of a wide range of materials, including textiles, plastics, wood products, and composites. It works by exposing a small sample of material to a controlled heat flux and measuring various parameters such as the heat release rate, mass loss rate, and smoke production. The sample is typically placed on a metal plate and a conical heater is positioned above it. The heat flux is increased until the material ignites, and then the device measures the fire behavior of the material as it burns. In our study, we used the cone calorimeter heater to provide a controlled heat flux allowing us to quantify the response the intumescent coating to a fire exposure.

2.2.1.1 Test Setup

Our testing setup consisted of a cone calorimeter, with an adjustable conical heater on top and a base positioned below it, as seen in Figure 2.4. The position of the cone was adjusted such that the distance between the center of cone and the base with sample produced the desired heat flux on the heat flux gauge which was measured to be 110mm. Aluminum foil was placed as a white background was needed to record the intumescence on camera clearly. An optical camera was mounted on a stand which was adjusted to record the base. The clear glass which enclosed the cone heater allowed easy visual access. A paper grid of 5 mm lines was attached on one side of the glass enclosure for visual measurement of the coating expansion.

2.2.1.2 Test sample preparation

2.2.1.2.1 Intumescent coating

FlameOff Fire Barrier Paint was our chosen intumescent coating. As per the instructions specified by the manufacturer in the application guide, power stirring was required to thoroughly mix the coating. A slotted paddle mixer was used to mix the coating. The mixer was connected to a 12.7

mm cordless drill, and the other end was inserted in the coating bucket. The coating was mixed for 3 minutes at 300 rpm until a uniform, smooth and creamy texture was obtained.

Figure 2.4 Cone calorimeter: Adjustable conical heater and base

2.2.1.2.2 Wood substrate

Virginia pine boards were used in the cone calorimeter tests. Samples were cut in a size of 99 mm by 99 mm which was the due to the size of metal pan being 102 mm by 102 mm. The thickness of the samples was 19 mm. The thickness of wood substrates was kept constant as in the cone calorimeter tests only the coating expansion relation was to be found. Two holes of size 2.38 mm were drilled on one side for thermocouples to be inserted later. They were drilled to half the substrate length as we wanted to measure the temperature at the center. The dimensions and locations of the drilled holes can be seen in Figure 2.5. The distance between the holes was fixed and decided by the slots on the metal pan, in which the sample would be placed later. The moisture content of the wood substrate was measured using a moisture meter to be 10%. General pin type Moisture meter with 0.1% accuracy was used. Self-adhesive polyimide fast response surface thermocouples were then attached to the top surfaces of each of the wood substrates to measure the temperatures at the wood-coating interfaces. These samples were then ready to be coated.

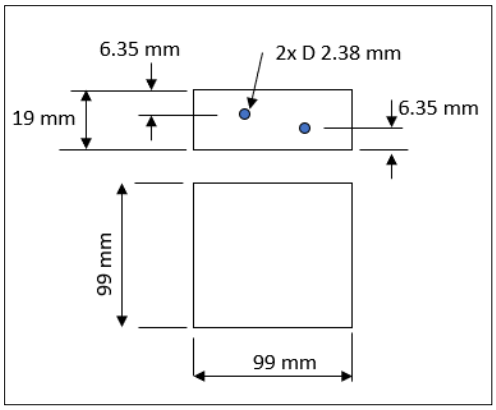

Figure 2.5 Dimension of test sample wood substrate

2.2.1.2.3 IC-wood substrate sample

Before the application of coating the samples were measured across different points along their lengths using a vernier caliper to find the average initial wood substrate thickness without the coating.

Wet film thickness (WFT) is a measure of the thickness of wet paint or liquid based coating, and it is monitored using a Wet Film Thickness gauge or comb as seen in Figure 2.6 with the WFT between the teeth 3 and 4. Dry Film Thickness is a measure of the thickness of an applied coating once it has cured. It should be checked once the product has dried, using a calibrated Dry Film Thickness gauge. The manufacturer had specified that this intumescent coating was 70% solids by volume. Thus, the conversion between the two was DFT = WFT x 0.70. The DFT for our tests was determined based on the recommended DFT in the coating specification guide (a minimum of 30 mil DFT for wood). Therefore, to understand the DFT scaling on fire exposure, we decided to test DFTs given in mm (mil) in five tests 0.12 (5), 0.25 (10), 0.51 (20), 1.02 (40) and 2.03 (80). The paint thickness is usually specified in mil which is measured in thousandths of an inch. (1 mil = 0.001 in.).

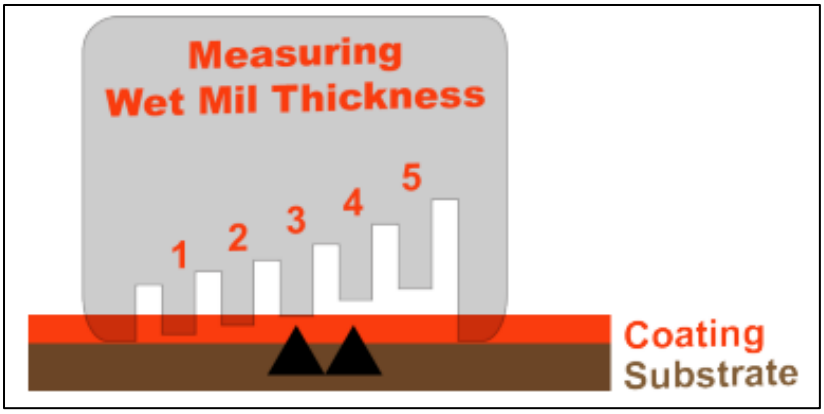

Figure 2.6 WFT measurement with WFT comb

The application guide recommended that the intumescent coating be applied with an airless paint spray or paint brush but not paint roller. A paint brush was employed in our study because the thickness per coat for the spray was specified to be 0.51 mm (20 mil) – 1.14 mm (45 mil) WFT, a value greater than our smallest coating thickness. Care was taken to evenly distribute the paint over the surface by using a crisscross motion; brushed from side to side and then up and down. The test samples were then left to dry without external stress for 48 hrs. A cured test sample is shown in the Figure 2.7.

Figure 2.7 Cured test sample with surface thermocouple attached

Once prepared, the samples were measured again at multiple locations to find the average coated wood thickness. Based on the difference between the initial and final readings, the actual dry film thickness was measured in each case. As seen in the Table 2.1, the measured DFTs matched well with the desired test sample DFTs. Apart from the 0.13 mm (5 mil) sample, the rest of the samples

are close to the desired DFT. The reason for the high error in 0.13 mm (5 mil) sample was the brush used had a minimum DFT of around 0.18 mm (7 mil) per coat.

Table 2.1 Measured Dry Film Thicknesses (DFT)

Test	Desired DFT		Measured DFT		Relative Error %
	(mil)	(mm)	(mil)	(mm)	
1	5	0.127	7.8	0.201	56
2	10	0.254	10.9	0.277	9
3	20	0.508	17.8	0.454	11
4	40	1.016	42.9	1.091	7
5	80	2.032	77.8	1.978	2

2.2.1.3 Instrumentation

The temperature was measured at the center of the plate for each test at 1/3rd and 2/3rd depth along the sample thickness. Two Omega high temperature low drift thermocouple probes, Type K, grounded with a probe diameter of 2.38 mm. were inserted at the positions marked by TC1 and TC2 shown in Figure 2.8. As seen before in Figure 2.7, one surface thermocouple had already been inserted during the sample preparation. A 2nd self-adhesive surface thermocouple was attached to the test sample at the bottom. Both were Omega self-adhesive polyimide fast response Type K surface thermocouples. The locations of the surface thermocouples were STC1 and STC2 respectively. The four thermocouples were attached to a datalogger, and the temperature measurement was gathered instantaneously using a LabView program.

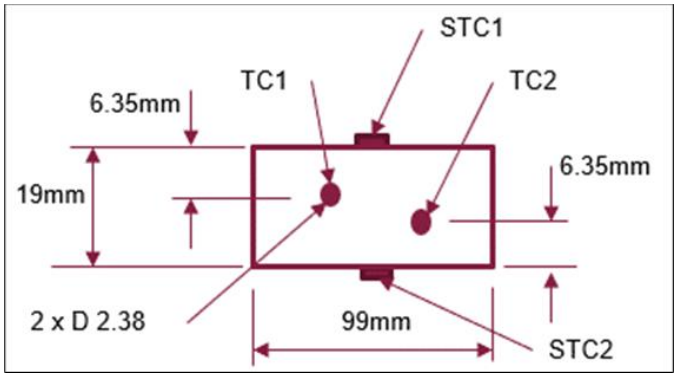

Figure 2.8 Location of thermocouples (TC) and surface thermocouples (STC)

The coating expansion was recorded on video by a camera mounted on a stand. Videos recorded were image processed in MATLAB.

2.2.1.4 Procedure

At the start of the test, the conical heater was turned on and the heat flux was brought to a constant value of 45 kW/m^2 as measured by a 12.5 mm diameter Medtherm Schmidt-Boelter heat flux gauge with a 0-100 kW/m^2 range. The correlation between the heat flux and the heat flux gauge voltage reading had already been tabulated before. The heat flux gauge measured the voltage to be 7.8 mV which corresponded to 45 kW/m^2. The gauge tip was placed at the center of the base and at an appropriate distance from the conical heater base such that this distance would equal the distance between the inserted pan-test sample exposed surface and the conical heater. Thus, 45 kW/m^2 would be the heat flux at the center of the test samples. This heat flux value was decided based on the recommendations made in past studies examined in the literature review.

Once the heater reached steady-state at the desired value, the test sample with the two surface thermocouples attached was placed in a metal pan. Ceramic fiber insulation was placed inside the metal pan before placing the test sample such that the bottom of the test sample was an insulated boundary condition. The sides of the pan were not insulated. The metal pan had two slots on its side and a square extension at its bottom which allowed it to be placed on the base of the cone calorimeter with no movement despite vibrations.

The thermocouple probes were inserted into the holes aligned with those slots. The camera started recording at this point. This metal pan-test sample was then placed on the base and four thermocouple end connectors were supported by the fixture supports as seen in Figure 2.9. The initial exposed surface was measured on the paper grid.

The tests were run for one hour or to ignition. The temperatures were recorded on the LabView program in real time throughout the test period. The coating expansion was measured visually on the paper grid at periodic intervals. Once the end time was reached, the conical heater was deactivated, thermocouples were detached, and the specimen was swiftly taken out of the heater to avoid additional exposure.

Figure 2.9 Test sample with metal pan placed on base

One-hour videos were recorded for each test. The video was trimmed to exclude the thermal bending and char decay in both wood and coating towards the end. This trimmed video was then converted into an image sequence using MATLAB. These images were then converted into shades of red and gray with image thresholding. Finally, the shades of gray are binarized to black and white and shades of red are converted to red (FF0000). The expansion was measured in pixels which was converted to mm. A green line shows the maximum expansion as seen in Figure 2.10. The conversion was based on the known length and thickness of the pan. The maximum expansion of the intumescent coating and the time to reach the maximum expansion was recorded.

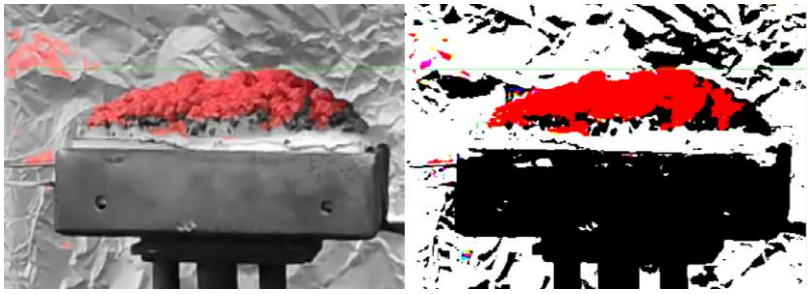

(a) (b)

Figure 2.10 Image processing (a) Gray and red image after thresholding and (b) Binarized gray to white and black with shades of red converted to red (FF0000).

2.2.2 Furnace testing

A sequence of thermal-only fire exposure tests at various scales was performed on our small-scale furnace to assess the effectiveness of our thermal scaling laws in practice.

2.2.2.1 Test setup

The furnace setup used for the previous fire exposure tests on wood in [2] was also used for our tests. The furnace consisted of a Unistrut frame with four propane burners and a ceramic fiber insulated barrier to safeguard the instrumentation from heat exposure, as illustrated in Figure 2.11b. The lower frame was built from 41 mm (1-5/8") Unistrut channels, measuring 1219 mm tall, 337 mm wide, and 692 mm tall. Three Unistrut members were positioned midway along the frame in the longitudinal direction to provide lateral bracing and hold the propane burners securely. The furnace utilized four Venturi-type 147 kW portable torch-style gas burners mounted vertically to heat the sample directly. Each burner had a flame diameter of approximately 152 mm, allowing for even distribution of temperature when four burners were spaced evenly over the sample surface. The burners were installed 305 mm beneath the sample surface to avoid direct contact with the sample surface and to instead heat the gas layer below the sample.

The top section of the fixture, where the sample was placed, was shielded by a 16 mm thick Type X gypsum wallboard thermal barrier wrapped on both sides with a 25 mm (1") ceramic-fiber insulation blanket of 128 kg/m^3 density, providing a total of 51 mm insulation. An opening was made in the barrier to reveal just the sample surface, which measured 610 mm by 140 mm. The temperature of the furnace gas was recorded using five Inconel-sheathed 1.5 mm diameter thermocouple probes positioned near the sample surface, as illustrated in Figure 2.11e.

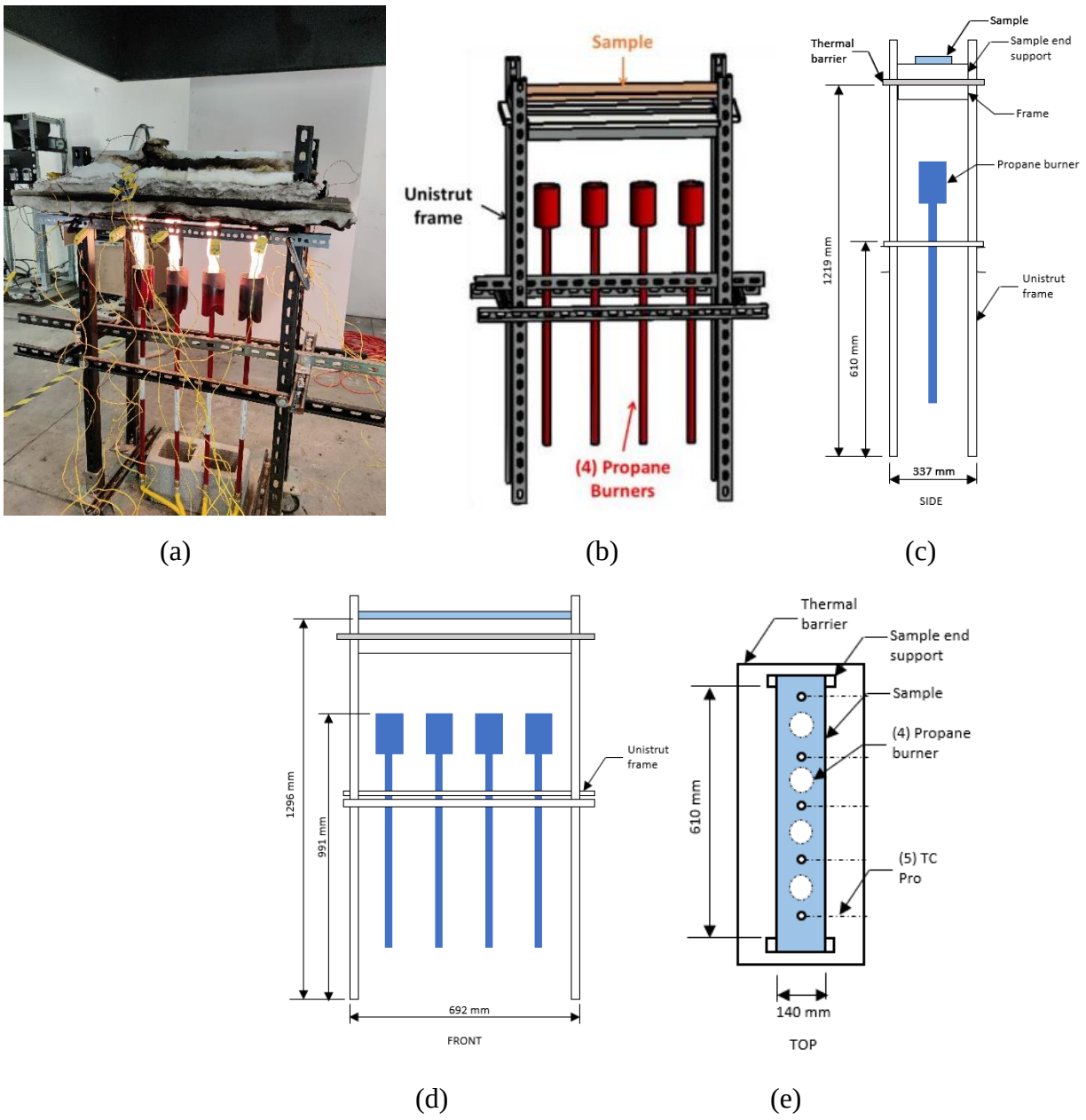

(a) (b) (c)

(d) (e)

Figure 2.11 Furnace test setup (a) Furnace test running (b) Unistrut frame, propane burners, and sample placement from literature [2] **(c) Side view displaying the elevation of burner mounts (d) Front view showing thermal barrier (e) Top view highlighting burner spacing and thermocouple positions beneath the opening**

2.2.2.2 Test sample preparation

2.2.2.2.1 Intumescent coating

The coating was prepared in the same way as mentioned in same as in section 2.2.1 for cone calorimeter test sample preparation.

2.2.2.2.2 Wood-substrate

Virginia pine boards were used in the furnace tests. Samples were cut in a size of 140 mm x 686 mm to fit the already existing furnace. The thicknesses of the test samples were 19 mm, 38 mm, and 76 mm for the ¼, ½ and full-scale tests respectively. We glued 19 mm thick wood boards together to make the 38 mm and 76 mm thick samples using Titebond III wood glue. As seen in Figure 2.12a, the glued samples were clamped at the ends and along the length. The sample was then allowed to dry overnight. The moisture content of the wood substrate was measured using a moisture meter to be 10.5%. General pin type Moisture meter with 0.1% accuracy was used. Self-adhesive polyimide fast response surface thermocouples were then attached to the top surfaces of each of the wood substrates to measure the temperatures at the wood-coating interfaces as seen in Figure 2.12b. These samples were then ready to be coated.

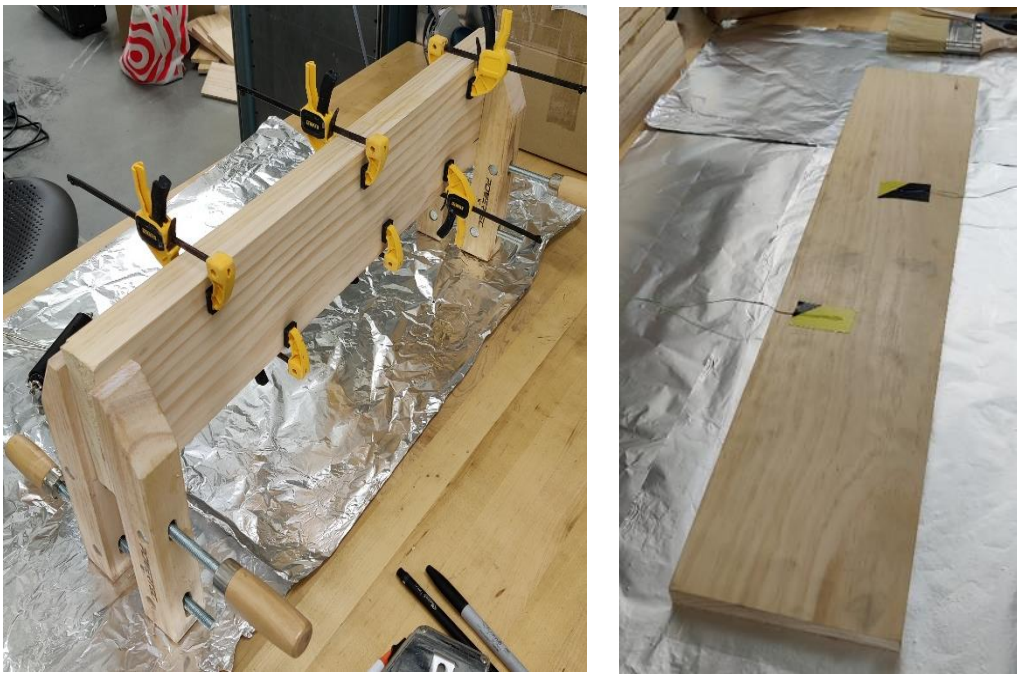

Figure 2.12 Wood substrate preparation (a) Clamped and glued sample allowed to dry (b) Surface thermocouples attached

2.2.2.2.3 IC-wood substrate sample

Before the application of coating, the thicknesses of the samples were measured at different points along their lengths using a vernier caliper to find the average uncoated wood substrate thickness. The coating process was the same as in Section 2.2.1. We used the relationship between Dry film thickness (DFT) and expansion obtained from the cone calorimeter tests to determine the target

DFTs for the furnace tests. The DFTs and their corresponding wood substrate thicknesses can be seen in Table 2.2. As seen from the scaling approach in Section 2.1, the coating thickness (in case of intumescent coating the final coating thickness after expansion) was to be scaled same as the wood substrate thickness. Based on the intumescent coating expansion relationship identified in cone calorimeter tests, the Dry Film Thicknesses (DFT) for each test sample was found out. For the DFTs identified, it meant that the final coating thickness after expansion would scale as χt. We also prepared a ¼ scale test sample at the DFT recommended by the coating manufacturer to compare with the expansion at low DFT value of 0.2 mm (8 mil).

Table 2.2 Furnace test sample dimensions

Test	Scale (χ)	Dry film thickness (DFT) expected		Wood substrate thickness	Expanded final coating thickness predicted (χ t)
		(mil)	(mm)	(mm)	(mm)
1	Quarter (1/4)	8	0.20	19	10 (1/4 t)
2	Half (1/2)	21	0.53	38.1	20 (1/2 t)
3	Full (1)	164	4.16	76.2	40 (t)
4	Quarter (1/4)	30	0.76	19	23 (1/2 t)

The coating was applied as seen in Figure 2.13. To prevent flames from penetrating towards the unexposed side from the sample edges during the furnace tests, the coating was also applied to the edges. The samples were allowed to dry for 48 hours as recommended by the coating manufacturer.

Figure 2.13 Intumescent coated wood test sample

The location of drilled holes for thermocouples is shown in Figure 2.14. After drilling, the test samples were prepared. The samples once prepared, were measured again, across different points along their lengths using a screw gauge to find the average wood-substrate thickness, now with the coating. Based on the difference between the initial and final readings, the actual dry film thickness was measured in each case. As seen in the Table 2.3, the measured DFTs matched well with the desired test sample DFTs.

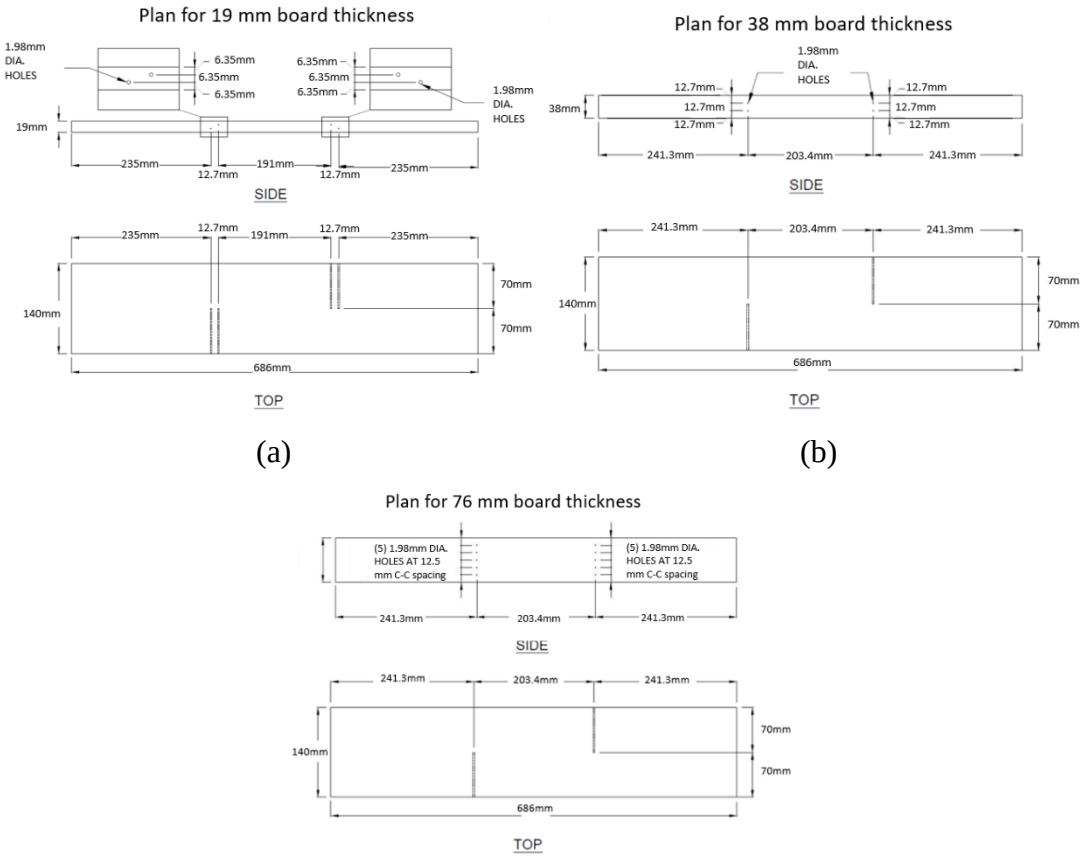

Figure 2.14 Drilled holes location in test samples (a) ¼ scale (b) ½ scale (c) Full scale

Table 2.3 Measured Dry Film Thickness (DFT) for test samples

Test	Desired DFT		Measured DFT		Relative Error %
	(mil)	(mm)	(mil)	(mm)	
1	8	0.20	8	0.20	1
2	21	0.53	20.1	0.51	4.2
3	164	4.16	156.7	3.98	4.5
4	30	0.76	30.30	0.77	1

2.2.2.3 Instrumentation

Furnace gas temperature was recorded using five Inconel-sheathed 1.5 mm diameter Type K thermocouple probes. The average gas temperature was manually controlled by adjusting the gas

flow rate in the burners with an Alicat MC-100 mass flow controller through a LabView interface. The gas temperatures were measured instantaneously using the LabView program.

The thermal response was quantified through temperature measurements. These measurements were recorded at the center of each sample, 70 mm from the longer sides, and at two redundant locations 241 mm from the short side ends, to avoid edge effects. Consequently, there were two sets of temperature data for each sample. 76 mm thick samples had five probes at each of the two locations. While 38 mm and 19 mm thick samples had two probes at each of the two locations. Omega high temperature low drift thermocouple probes, Type K, grounded with a probe diameter of 1.57 mm were inserted to measure the depth temperatures. As seen before in Figure 2.12b, two surface thermocouples had already been inserted during the sample preparation (exposed side). Two surface thermocouples were also attached to the bottom (unexposed side) for each of the test samples. Omega self-adhesive polyimide fast response Type K were used as surface thermocouples. All gas temperatures and sample temperatures were recorded using a LabView program at a frequency of 60 Hz.

2.2.2.4 Procedure

Four fire exposure tests were carried out using the reduced scale furnace. When preparing the test samples, it was presumed that the primary mode of heat transfer occurred through the thickness of the sample. Consequently, all samples had identical lengths and widths. The scaling was determined solely by the sample thickness.

Samples were positioned on the furnace frame over the opening, exposing the central 610 mm. The furnace's remaining surface area not covered by the samples was obstructed with Type X gypsum wallboard barriers insulated with a 51 mm ceramic-fiber insulation blanket. To prevent flames from penetrating the sample's edge and ensuring heat transfer occurred solely through the sample's thickness, a ceramic-fiber insulation blanket was placed on the sides of the samples.

The experiments concluded after subjecting the samples to fire exposure for a duration equivalent to one hour at full-scale. According to the Fourier number scaling laws, the corresponding times

for full-scale, 1/2-scale, and 1/4-scale were 3600 seconds, 900 seconds, and 225 seconds, respectively. The test matrix can be seen in Table 2.4.

After completion of the desired exposure time, the gas supply to the furnace was shut off, the thermocouples were detached, and the sample was promptly taken out of the furnace to avoid additional exposure. Following this, the char depth of the exposed samples was assessed. The final thicknesses were measured at various points along their lengths using a vernier caliper to determine the average wood-substrate final thickness, now including the expanded coating. The actual coating expansion in each instance was measured based on the difference between the initial and final readings.

Table 2.4 Test matrix for furnace fire exposure tests

Test	Exposure Scale (χ)	Scaled E119 duration	DFT	Sample width	Sample thickness	Sample length
		(s)	(mil)	(mm)	(mm)	(mm)
1	Quarter (1/4)	225	8	140	19	610
2	Half (1/2)	900	20	140	38	610
3	Full (1)	3600	157	140	76	610
4	Quarter (1/4)	225	30	140	38	610

2.3 Results

2.3.1 Cone tests

The objectives of the cone calorimeter tests seen in Section 2.2 were an initial assessment of expansion of the intumescent coating (IC) for scaled dry film thicknesses (DFTs) under a constant heat flux and identifying the DFTs required for the furnace tests.

As shown in Figure 2.15 the intumescent coating expanded to different thicknesses depending on the initial DFT. Of the five tests with DFTs given in mm (mil) 0.12 (5), 0.25 (10), 0.51 (20), 1.02 (40) and 2.03 (80), all coatings except for the 0.12 mm (5 mil) coating sample expanded to a noticeable thickness. The 0.12 mm (5 mil) was much thinner than the recommended coating

thickness of 0.76 mm (30 mil) and did not show expansion. Thus, it was excluded while finding an intumescent coating expansion relationship.

Figure 2.15 Intumescent coating after expansion clockwise from top left 2.03, 0.51, 1.02 and 0.25 mm

Using the data for the expansion of the obtained from the image processing, we obtained the expansion rate and final thickness for each initial DFT. The comparison of result between different tests is shown in Figure 2.16. Final expansion thicknesses are marked on the plots. Initially the rate of expansion was observed to be the same for the first 60 seconds. However, the expansion rate changes after that period, depending on the initial DFT as seen by the curves flattening at different rates. It is also noted that the flatter part of the curve increases in size as the DFT increases. Thus, the time to reach the maximum coating thickness increases with increasing DFT.

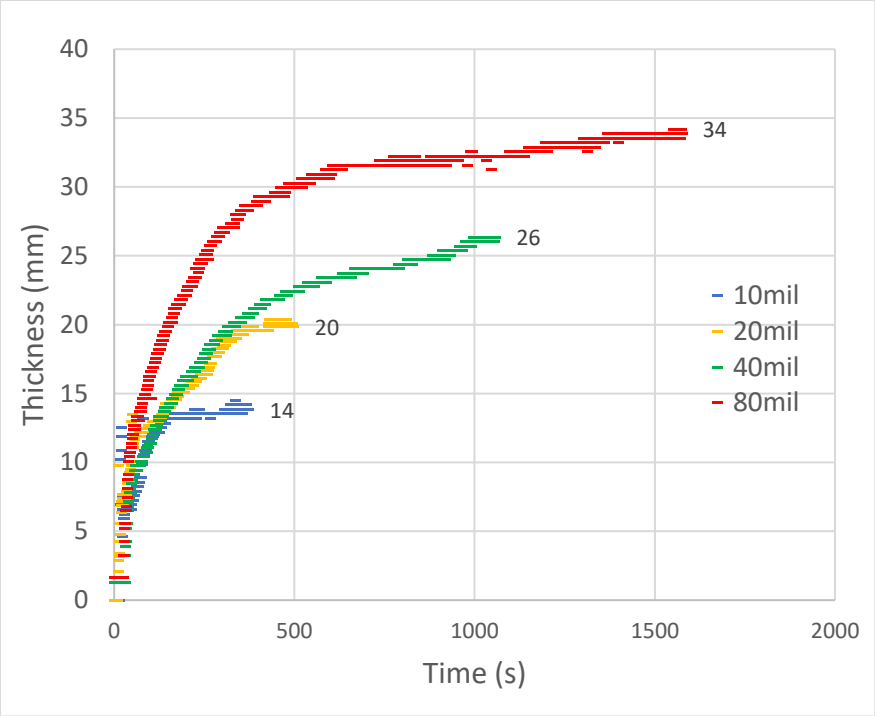

Figure 2.16 Rate of expansion in intumescent coating at 45 kW/m^2

We obtained the final thicknesses of the intumescent coatings after expansion as an output from the image processing done in MATLAB. As explained above test 1, which was a 5 mil DFT was excluded. Based on their initial dry film thicknesses (DFT) and the final expanded thicknesses, the expansion ratio was calculated. As shown in Table 2.5 contrary to the constant expansion thickness assumed in many numerical models [10] [42] [43] the expansion ratio of the intumescent coating depends on the DFT and decreases as the initial DFT increases.

Table 2.5 Final thicknesses after intumescent coating expansion

Test	DFT (mm)	Final thickness (mm)	Expansion ratio
2	0.28	14	50
3	0.45	20	42
4	1.10	26	24
5	1.98	34	17

Now, based on this expansion seen in the cone calorimeter, we wanted to identify the DFTs required for the furnace tests. Based on the four sets of data points as shown in Figure 2.17, we obtained the following empirical relationship

$$t_f = 9.8106ln(t_i)+25.949 \quad (2.5)$$

where, t_f is final expanded thickness and t_i is initial DFT.

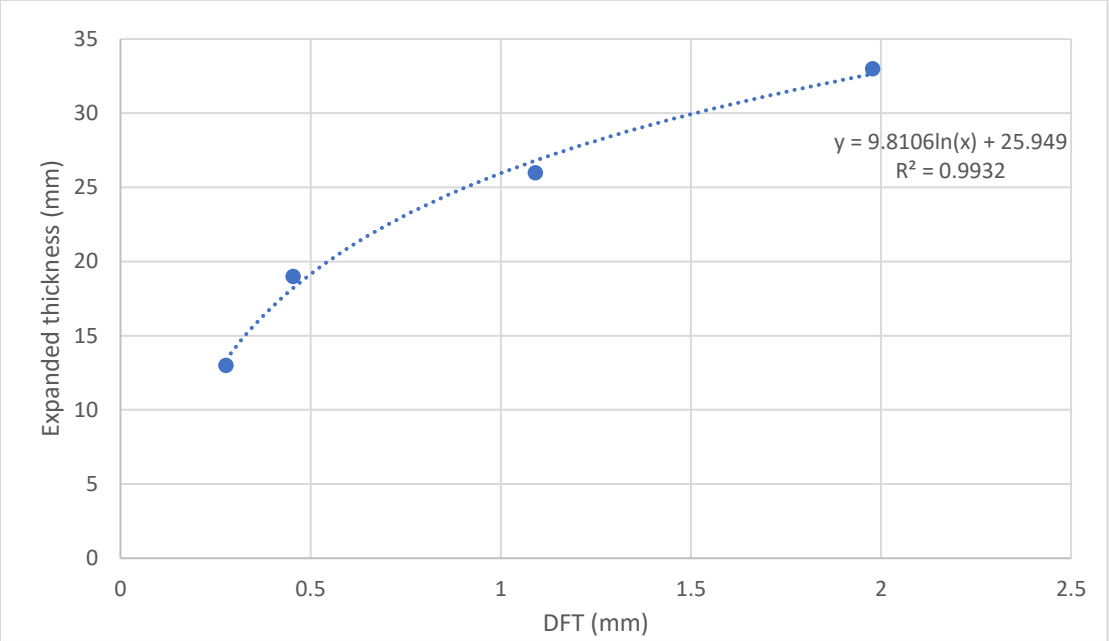

Figure 2.17 Relationship developed between expanded coating thickness and initial dry film thickness

Using this relationship, we selected the final expanded thicknesses to be 40 mm, 20 mm, and 10 mm for the full, ½ and ¼ scale furnace tests, respectively. Ideally, we would have chosen 60 mm, 30 mm, and 15 mm. However, the 60 mm expanded thickness would have required a DFT greater than we could successfully apply. The range of 40 mm to 10 mm was employed because all 3 of the values were near or within the range over which the relationship had been experimentally measured and shown to be achievable.

As discussed previously, the time to reach the maximum coating thickness was seen to increase with increasing DFT as shown in Figure 2.16. Hence, our assumption of instantaneous coating expansion as mentioned in the scaling methodology in Section 2.1 was not correct for higher DFTs. As we had chosen 20 mm and 40 mm for half and full-scale furnace tests, it was important to identify the time it would take to reach the desired thicknesses. The 10 mm (¼ scale test) DFT was

small enough to still be considered instantaneous. Based on the four sets of data points for expansion thickness and time to reach that thickness, we developed a relation as shown in Figure 2.18. Based on this relation we looked at the times it would take for the coating to reach 20 mm (½ scale) and 40 mm (full scale). It would take half of the total test time for both full and half scale tests to reach the maximum coating thickness after expansion as shown in Table 2.6. For the ¼ scale test the predicted time to reach maximum thickness was less than one-third of the test time.

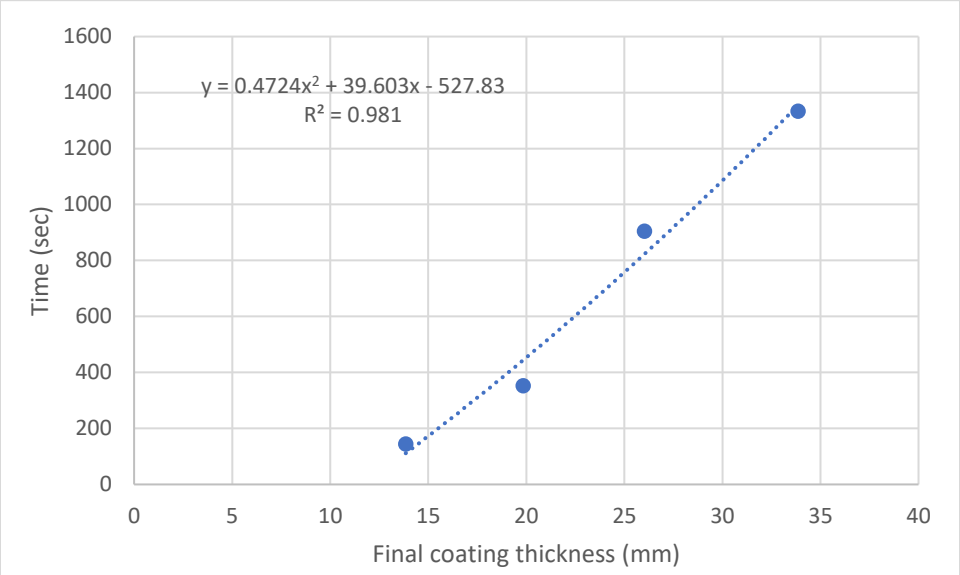

Figure 2.18 Predicted time to reach final coating thickness after expansion

Table 2.6 Predicted time taken for furnace test DFTs to reach complete expansion

Scale	Final thickness (mm)	Test time (T) (sec)	Time for expansion (Te) (sec)	Te/T
Full	40	3600	1812.13	0.503
Half	20	900	453.19	0.503

Our assumption of instantaneous coating expansion was not correct. Since our interest in expanded thickness was related to the thermal conductivity through it, it made sense to investigate the difference between the average coating thickness and the final expanded coating thickness. We calculated the average coating thicknesses for the four Tests 2 - 5.

Table 2.7 Time averaged means vs the final thicknesses for the intumescent coating

Test	Final thickness (mm)	Time averaged thickness (mm)
1	No data	No data
2	13	11
3	19	15
4	26	20
5	33	29

From the Table 2.7 we see that the average coating thickness was not significantly different from the final thickness for all tests. Therefore, for our furnace tests, we considered the assumption of instantaneous coating thickness while deciding on the test sample dry film thicknesses. From the dry film thickness (DFT) and the final expanded thickness relationship developed, we found the test sample matrix as shown previously in furnace test procedure in Section 2.2.2. Thus, the objectives of the cone calorimeter tests were satisfied.

2.3.2 Furnace tests

The objective of the furnace tests was to find the extent to which the intumescent coating can be scaled maintaining the thermal similitude in scaled lumber as seen in Section 2.2. First, we looked at the input furnace gas temperature curves for each test and compared them with the desired fire curves at each scale. The comparison is shown in Figure 2.19 where the average gas temperatures are calculated from the five thermocouples measuring the furnace. The difference between the desired and actual area under the time-temperature curve was 2% for the first three tests and 6% for the fourth test. All the tests were within the 10% difference set by the ASTM E119 standard.

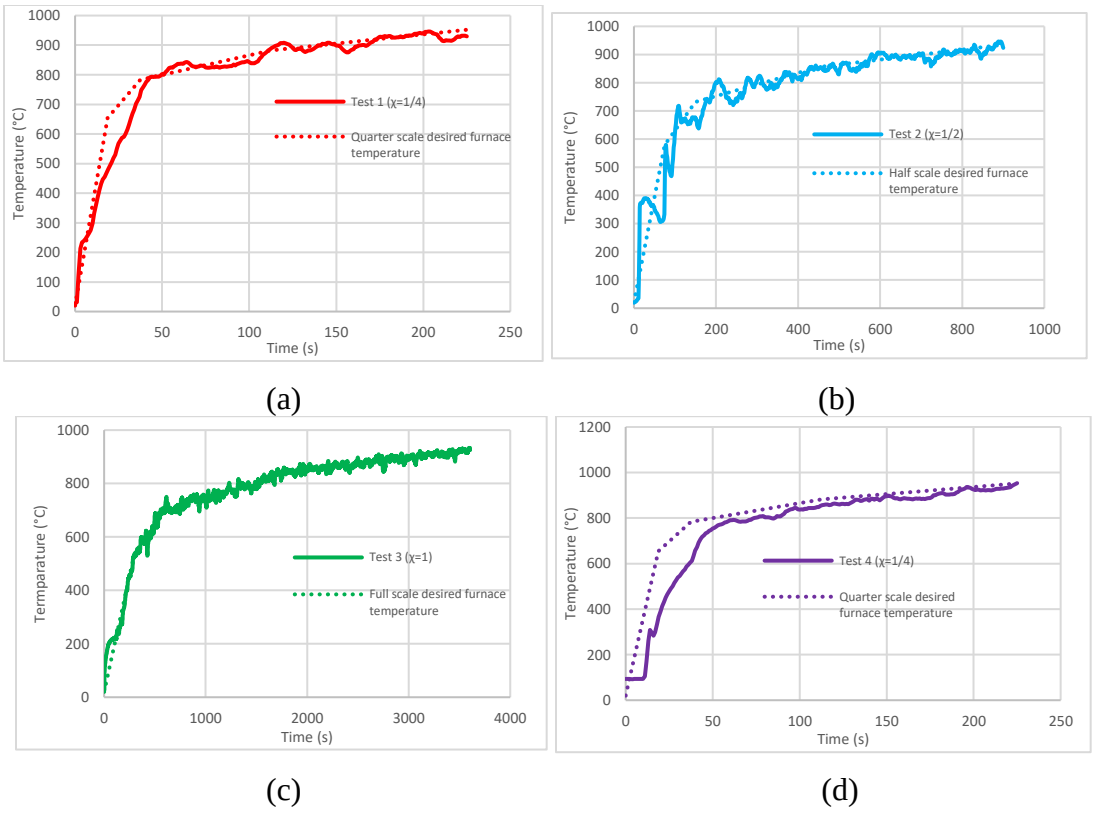

Figure 2.19 Average furnace gas temperatures vs desired furnace temperature at (a) Quarter scale (0.2 mm DFT) (b) Half scale (c) Full scale (d) Quarter scale (0.76 mm DFT)

The intumescent coating expanded during the tests and the expansion was measured after the tests. Figure 2.20b shows that the coating expanded uniformly across the length for all tests in contrast to the coating expansion observed in the cone calorimeter tests, where the center of the sample had the maximum expansion. Also, the difference in thickness of the coating expansion is seen between full, ½ and ¼ scale.

(a) (b)

Figure 2.20 Intumescent coating expansion after the end of furnace tests (a) Top view (b) Side view

The final coating thickness was measured at different locations to find the average final expanded coating thickness for the four tests. Average coating thicknesses are tabulated in Table 2.8. Inspection shows that the final coating thickness in Test 2 is half of that in Test 3. Test sample's final coating thickness in Test 1, however, is not half of that in Test 2. Test 4 has nearly the same final coating thickness as that in Test 2.

Table 2.8 Final intumescent coating thickness after expansion at the end of furnace tests

Test	Scale (χ)	Average Dry Film Thickness	Average final coating thickness	
		(mil)	(mm)	(mil)
1	Quarter (1/4)	8	3.6	141
2	Half (1/2)	20	18	722
3	Full (1)	157	42	1667
4	Quarter (1/4)	30	18	739

The temperature gradient was measured for each test at uniform depth as seen by the thermocouple locations described in Section 2.2.2. If the temperature gradient versus time profiles for the ¼ and ½ scale test matched the full-scale test profile, a thermal similitude would be achieved between full, half and quarter scales and our scaling methodology would be successful. Figure 2.21 provides a comparison between the full-scale and ½ scale temperature gradients with full-scale effective time. The thermocouples on the exposed side to the furnace came off in few of the tests and hence temperatures at exposed side (Depth 0) were not added in the plot. The nature of the curves matches at each of the depths. Temperature curves match very well at depths (2/3)L and L. There is an approximate 20 °C gap between scales at depth (1/3)L. However, there exists a large uncertainty in measurement for full scale depth (1/3)L as shown in Figure 2.21a. Temperature measurements at depth L are wavy because unlike only conduction, a combination of conduction, convection and radiation affects the temperature at the unexposed side. Overall, there is a good agreement between the full and ½ scale temperature gradients with time (Test 2 and 3). Full and ½ scale plot where the maximum error was 25% at depth (1/3)L, the rest of the depths had low errors 10% and 18%.

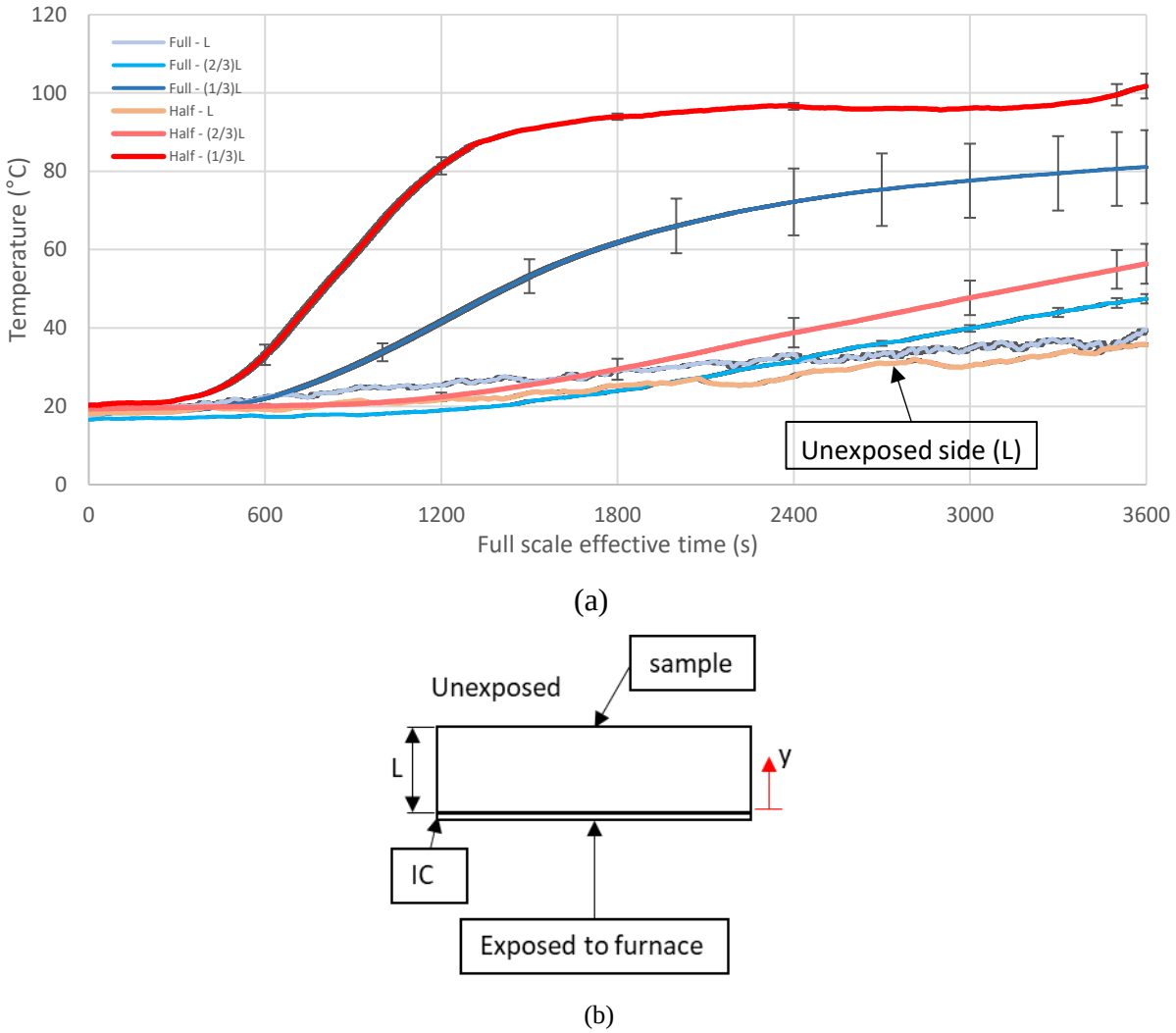

Figure 2.21 Temperature gradients in Full-scale vs. ½-scale (a) average with uncertainity (b) Depth coordinate location

However, temperature gradients don't agree well between the full and ¼ scale temperature gradients with time (Test 1 and 3). The plots are shown in Figure 2.22. Test 4 with 0.76 mm (30 mil) DFT for ¼ scale had a better agreement with full-scale Test 3 compared to 0.2 mm (8 mil) DFT Test 1 with Test 3.

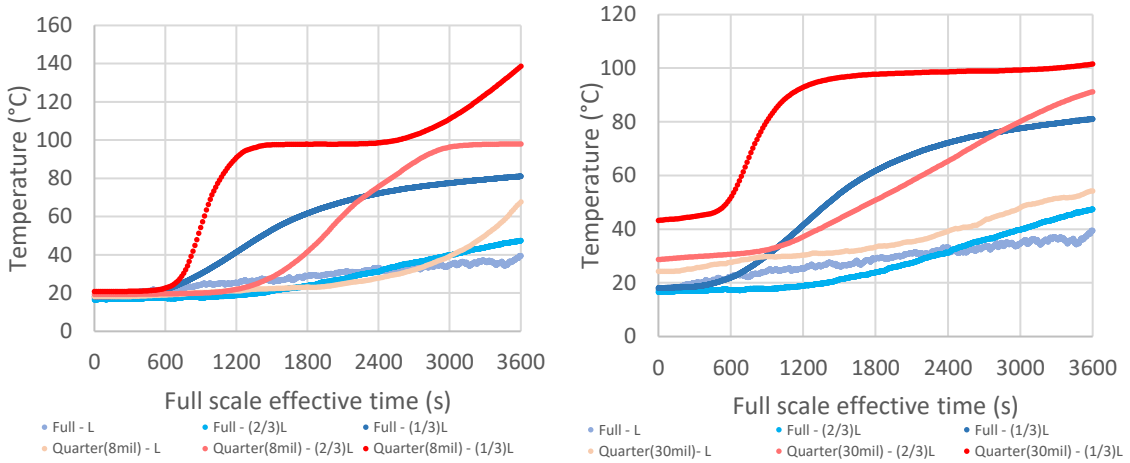

(a) (b)

Figure 2.22 Temperature gradients in Full-scale vs. 1/4-scale (a) 0.2 mm (Test 1) (b) 0.76 mm (Test 4)

2.4 Discussion

2.4.1 Scaling observed in intumescent coatings

The final coating thickness average value was measured for each of the sample after tests as seen in Section 2.3. Based on the expansion relation developed in cone calorimeter test, we had predicted the dry film thicknesses such that the final coating thicknesses would scale by χ. Table 2.9 shows the predicted and actual coating thicknesses measured after expansion. Full-scale (Test 3) and ½ scale (Test 2) actual thicknesses matched very well with the predictions. However, ¼ scale (Test 1) deviated 70% and ¼ scale (Test 4) deviated 21% from the predicted values.

Table 2.9 Predicted and actual coating thicknesses

Test	Scale (χ)	Predicted final coating thickness (mm)	Actual final coating thickness (mm)	Relative error %
1	Quarter (1/4)	10	3.6	70%
2	Half (1/2)	20	18	10%
3	Full (1)	40	42	5%
4	Quarter (1/4)	23	18	21%

From the ¼ scale Test 4 results, we see that 225 seconds is too short of time to reach the maximum expansion as predicted by the relation. Also, the developed relation (2.5) works well up to 0.51 mm (20 mil) DFT (predicted expansion thicknesses 15 mm), but the predicted final coating thicknesses deviates a lot from the actual coating thicknesses for lower DFTs like 0.2 mm (8 mil), as seen by Test 1 result. This is supported by expansion ratios seen in Table 2.10. Test 2, Test 3, and Test 4 expansion ratios decrease with increasing DFT like the trend observed in coating expansion ratios in cone calorimeter tests in Section 2.3.1. Test 1 sample did not reach the maximum expansion possible.

Table 2.10 Coating expansion ratios for furnace tests

Test	Scale (χ)	Average Dry Film Thickness (mm)	Average final coating thickness (mm)	Average expansion ratio
1	Quarter (1/4)	0.2	3.6	17
2	Half (1/2)	0.51	18	36
3	Full (1)	3.99	42	10
4	Quarter (1/4)	0.76	18	24

We can conclude the following:

1. Our developed relationship for intumescent coating expansion works for full and ½ scales.
2. Final coating thickness deviates a lot from the predicted values for ¼ scale due to limited time for expansion (225s) & low DFTs which are outside the expansion relationship range.

We saw previously in Section 2.3 the temperature gradient vs time comparison between full, ½ and ¼ scale tests. The temperature gradient comparison at full scale effective time of 3600 s is shown in Figure 2.23 (a) and (b). From this comparison and Figure 2.21 (a) the full and ½ scale temperature gradients matched well. Test 1 ¼ scale 0.2 mm (8 mil) DFT did not match well with full-scale Test 3 as seen previously in Figure 2.22 (a) and Figure 2.23 (a). But if we replaced ¼ scale 0.2 mm (8 mil) with 0.76 mm (30 mil) as DFT we observed better agreement with full-scale as seen in Figure 2.22 (b) with time and in Figure 2.23 (b) at full scale effective time of 3600s. At the unexposed end (y=L), we saw a relative error of 9% between ½ and full-scale temperatures. However, ¼ (0.2 mm) and full-scale have a very large error of 70%. The expansion error between

predicted and actual final thickness which was also 70% as seen in Table 2.9. Thus, the time restricted limited expansion in ¼ (0.2 mm) Test 1 resulted in no thermal similitude between full and ¼ scale (0.2 mm). Increasing the DFT in ¼ scale improved the thermal response scaling between full and ¼ scale as the relative error between ¼ and full-scale temperatures reduce to 36% from 70% but it was still high. Therefore, the developed relation (2.5) can be used to accurately scale down to ½ scale while maintaining thermal similitude. However, to get better results while scaling to ¼ scale, it is recommended to use DFT of ½ scale at ¼ scale to compensate for limited expansion due to time and heating rate differences.

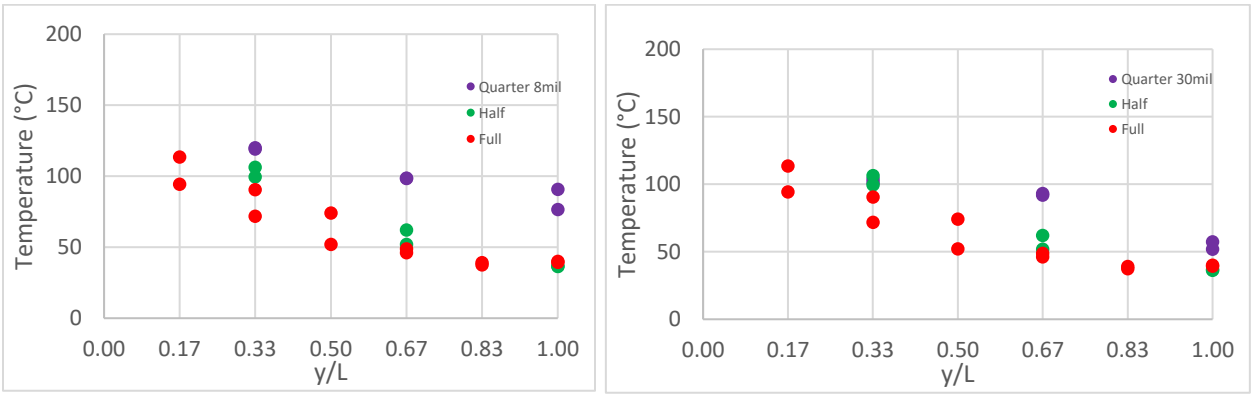

(a) (b)

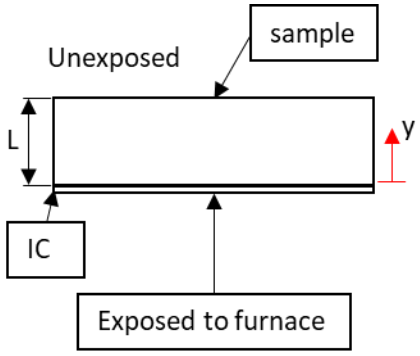

(c)

Figure 2.23 Temperature variation along the depth at full scale effective time 3600 s (a) with ¼ 0.2 mm (8 mil Test 1) (b) with ¼ 0.76 mm (30 mil Test 4) (c) Depth coordinate location

Thus, we can conclude that

1. Thermal similitude observed between ½ scale and full-scale and that the scaling works well from full to ½ scale.

2. No thermal similitude observed between full and ¼ scale due to the observed coating expansion not being according to the developed expansion relationship.
3. The final coating thickness in the case of ¼ scale must be increased to the half scale final thickness to maintain thermal similitude.

The developed methodology was tested for one commercial intumescent coating. The importance of developing this methodology is that there is a possibility that the same scaling cannot be used for other types of intumescent coatings. Due to differences in formulations, the expansion relations might be different for different intumescent coatings. This methodology can be used to develop a scaling relationship for other commercially available intumescent coatings, and other types of fire-resistant coatings, like MgO based coatings.

2.5 Summary

A methodology used to scale ASTM E119 fire resistance test for dimensional lumber was updated to cover fire resistant coated wood. The first step was deciding on the coating thicknesses needed for full, ½ and ¼ scales. With the aim of maintaining a thermal similitude between different scales, the coating thicknesses in full, ½ and ¼ scale were found to scale by a factor of χ when scaling the time by a factor of χ^2 to keep the Fourier number constant across scales. This developed methodology was tested on a commercially available intumescent coating, a type of coating which expands when exposed to fire. An additional step was required for this coating. Tests were done on cone calorimeter to identify a relation between final coating thickness and initial dry film thickness (DFT). Finally, furnace tests were performed on three scales full, ½ and ¼ by exposing the samples to thermal only loading. Thermal similitude was observed between full and ½ scale. Thus, the methodology successfully worked for scaling from full to ½ scale. This will reduce the test times by a factor of 4. However, thermal similitude was not observed between full and ¼ scale. For this coating, it appears that the DFT at ½ scale should also be used at ¼ scale. Additional testing on different coatings needs to be performed to assess whether this approach should be used for other intumescent coatings.

Chapter 3 Joints

The fire resistance of wood-based structures is of utmost importance in the construction industry, particularly in the design and implementation of safe and sustainable buildings. One critical aspect of wood-based structures is the performance of joints under fire exposure, as joints play a pivotal role in the overall structural stability and load-bearing capacity. Various types of joints, such as half-lap, dovetail, mortise, and tenon, have been used in wooden structures to connect different components. These joints play a crucial role in the load-carrying capacity and overall stability of a structure under fire conditions. This chapter focuses on the fire resistance of wood-based half-lap joints, which are commonly used in timber frame constructions due to their simplicity and effectiveness in load transfer. In future, this can be extended to cover other types of joints.

Half-lap joints consist of two overlapping members, with each member having half of its thickness removed at the joint location. This configuration allows for increased contact area between the members, leading to a more uniform distribution of stress and improved load-bearing capacity. However, the performance of these joints under fire conditions has not been extensively studied, and there is a need to better understand their behavior under combined thermo-structural loading. In this chapter, we will investigate the fire resistance of wood-based half-lap joints using the scaling methodology developed and validated in previous study for fire-resistant coated wood and adapt it for wood based half-lap joints. We will begin with the scaling approach for half-lap joints, followed by a comprehensive analysis of the experimental setup, results, and validation of the scaling laws on half-lap joints.

3.1 Scaling approach

Like the scaling approach in Section 2.1, we used scaling methodology for thermo-structural tests developed in the previous study [2], combining uniform geometric scaling, Fourier number time scaling, boundary condition alignment with structural scaling. The uniform geometric scaling meant that when an object underwent uniform scaling, it became a smaller version of the original, with similar geometric characteristics. The degree of scaling was determined by the uniform scaling factor, denoted by χ, which represented the ratio of the reduced-size dimensions to the full-size dimensions. For example, a half-scale test corresponded to χ = 0.5. illustrated the original

assembly, which had width b, length L, and thickness d. To preserve structural similarity, the scaled assembly had to have dimensions that were proportional to those of the original, when subjected to the same load per unit area p. Subscripts 1 and 2 denote full scale and reduced scale dimensions, respectively.

$$L_2 = \chi L_1 \tag{3.1}$$

$$b_2 = \chi b_1 \tag{3.2}$$

$$d_2 = \chi d_1 \tag{3.3}$$

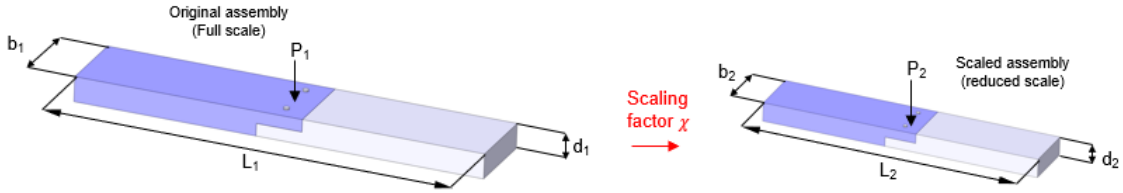

Figure 3.1 Assessment of dimensions between the original and scaled test for a sample subjected to three-point bending

3.1.1 Thermal scaling

To replicate the thermal behavior, scaling laws integrate Fourier number time-scaling with boundary condition alignment. A concise overview of these scaling laws is presented below. When the specimen's thickness is diminished by a factor χ, it is necessary to implement time scaling to achieve similarity in the 1-D heat transfer across the specimen's thickness. The solution to the 1-D heat equation is governed by the Fourier number,

$$Fo = \frac{\alpha \tau_1}{d^2} = \frac{\alpha \tau_2}{(\chi d)^2} \Rightarrow \tau_2 = \chi^2 \tau_1 \tag{3.4}$$

Here, d denotes the thickness, α represents the thermal diffusivity, and t is a suitable characteristic time (e.g., the total test duration). As a result, Fourier number time scaling decreases the fire exposure time in the reduced-scale test by a factor of χ^2. Boundary condition was matched as specified by Gangi et al. in [2]:

> *"Boundary condition alignment ensures that the specimen's boundary condition on the furnace side, where the exposure takes place in this 1-D heat transfer, is preserved in the scaled test. The heat flux must remain consistent between the original and scaled tests to accurately scale the heat transfer process. The boundary condition on the exposed surface consists of both radiation and convection from the furnace fire curve. The temperature of the scaled test fire curve*

can be adjusted to provide the same heat flux as the full-scale tests. Full-scale furnace gas temperatures are defined by standard fire time-temperature curves, such as ASTM E119. At each time step, the modified furnace temperature must be computed to produce the same heat flux as in the full-scale test."

Boundary condition alignment calculated in [2] for ½ and ¼ scales is shown in Figure 3.2.

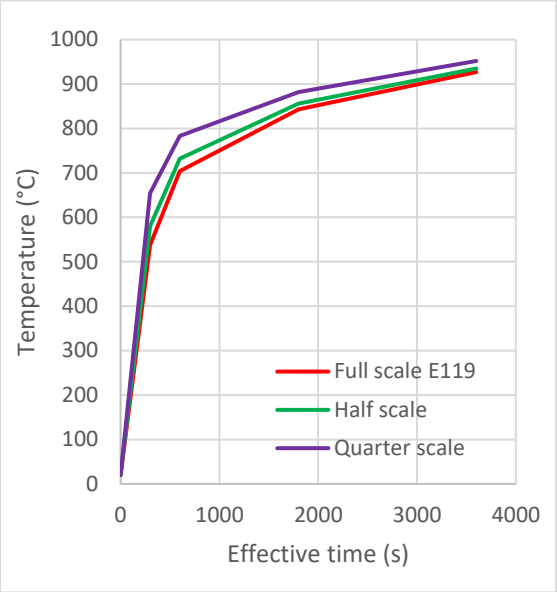

Figure 3.2 Fire curves at different scales from literature [2]

3.1.2 Structural scaling

Let's consider the original full-thickness assembly in a three-point bending scenario, featuring simply-supported end conditions with a static point load of P applied at the mid-span, which is $L/2$ from each support, as depicted in Figure 3.1. If the L/d ratio is sufficiently large, the failure mode becomes flexural, and bending stress dominates. The maximum bending stress, σ, resulting from the three-point bending of a sample is given by Eq. (3.5). To generate the same bending stress in a sample with reduced thickness, length and width, Eq. (3.8) indicates that the total applied load, P, must be decreased by a factor of χ^2. Additionally, three-point bending creates shear stress.

$$Bending\ stress\ -\ \sigma = \frac{3PL}{2b(d)^2} \tag{3.5}$$

$$\sigma_1 = \frac{3P_1L_1}{2b_1d_1^2} \tag{3.6}$$

$$\sigma_2 = \frac{3P_2L_2}{2b_2d_2^2}$$

From (3.1), (3.2) and (3.3)

$$\sigma_2 = \frac{3P_2\chi L_1}{2\chi b_1 \chi^2 d_1^2}$$

$$\sigma_2 = \frac{3P_2 L_1}{2b_1 \chi^2 d_1^2} \tag{3.7}$$

For equal bending stresses, from (3.6) and (3.7)

$$\frac{P_2}{P_1} = \chi^2 \tag{3.8}$$

As per Euler-Bernoulli beam theory [44], the maximum elastic deflection resulting from flexural stress at the mid-span of a rectangular beam is given by Eq. (3.9). When the thickness, length and width are scaled by χ and the load is scaled by χ^2, Eq. (3.9) reveals that the deflection should scale as a factor of χ.

$$\text{Deflection - } \delta = \frac{PL^3}{48EI_y} = \frac{PL^3}{4Ebd^3} \tag{3.9}$$

$$\delta_1 = \frac{P_1 L_1^3}{4Eb_1 d^3} \tag{3.10}$$

$$\delta_2 = \frac{P_2 L_2^3}{4E b_2 d_2^3}$$

From (3.1), (3.2) and (3.3)

$$\delta_2 = \frac{\chi^2 P_1 \chi^3 L_1^3}{4E\chi b_1 \chi^3 d_1^3}$$

$$\delta_2 = \frac{\chi P_1 L_1^3}{4Eb_1 d_1^3} \tag{3.11}$$

For equal bending stresses, from (3.10) and (3.11)

$$\delta_2 = \chi \delta_1 \tag{3.12}$$

The thermo-structural scaling laws introduced in this research rely on the premise that the heat transfer resulting from furnace fire exposure will predominantly occur in a 1-D manner through the thickness of the specimen.

3.2 Experimental approach

The objective was to showcase the application of thermo-structural scaling laws to wood-based materials exhibiting intricate behavior under fire exposure. Consequently, this experimental research will explore the extent to which the scaling laws applied to half-lap joints preserve comparable thermal performance and whether this translates to structural similitude across full and reduced scales.

3.2.1 Furnace testing

A sequence of thermal-only fire exposure tests at two scales was performed on our downscaled furnace to assess the effectiveness of our thermal scaling laws in practice. The objectives of the furnace tests were:

1. Evaluate the performance of scaled joint assemblies
2. Evaluate feasibility of scaling joints through a series of bench-scale furnace tests

3.2.1.1 Test setup

We used the same furnace design used for furnace tests on intumescent coated wood substrates in Section 2.2.2. However, previously we performed thermal only tests on the furnace. For thermo-structural tests on half-lap joints, we had to modify the test setup. Load was applied at the center of the unexposed side on the test sample on a loading bar. The 711 mm loading bar was made from 51 mm square steel tubing and had a self-weight of approximately 22 N, accounting for the uplift force in the string potentiometers. Additional loading was applied via weight plates stacked on the center of gravity of the loading bar, shown in as shown in Figure 3.3 (a). This addition to the test setup used in Section 2.2.2 was same as for thermo-structural tests in Ref. [2] for ½ scale test sample. However, as ¼ scale test sample was χ times smaller than ½ scale, we attached a new thermal barrier with smaller slot for fire input from the bottom. We also included in new end supports for the smaller sample length of ¼ scale shown in Figure 3.3 (b).

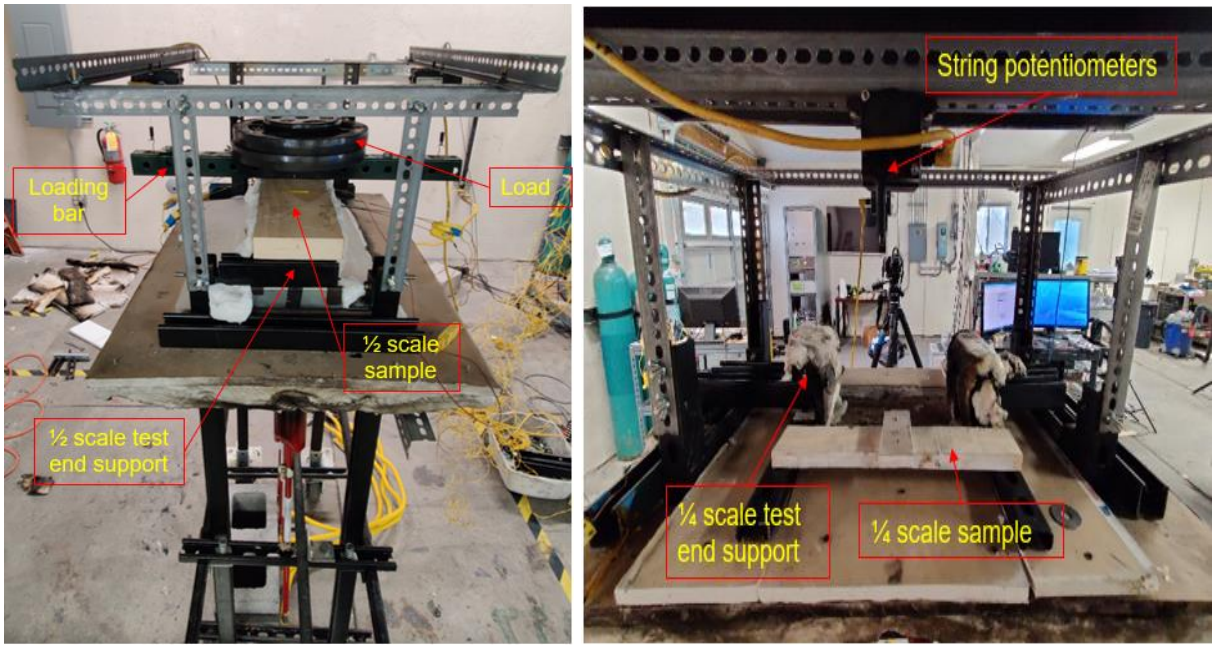

(a) (b)

Figure 3.3 Test setup modified for mechanical loading (a) ½ scale test (b) ¼ scale test

3.2.1.2 Test sample preparation

As in Section 2.2.2, Virginia pine boards were used in the furnace tests. Unlike in the previous test, lengths and widths of the samples were varied along with the thickness because of the structural scaling approach described in Section 3.1. This along with the maximum length and load supported by the existing test fixture restricted the tests to two scales - ½ and ¼. Samples were cut in a size of 140 mm x 686 mm which was made to fit on the already existing furnace setup for ½ scale test. For ¼ scale tests, samples were cut in 70 mm x 381 mm. The thicknesses of the test samples were 19 mm and 38 mm for the ¼ and ½ scale tests respectively. Because of the unavailability of 38 mm thick wood boards, we decided to glue 19 mm thick boards to create 38 mm thick halves of the half-lap joint for half scale using Titebond III wood glue. For ¼ scale, 19 mm wood boards were cut in machine shop to create 9.5 mm thick wood boards which were then glued to form 19 mm halves of half-lap joint to maintain the uniformity in sample preparation as of half-scale. The dimensions of the two halves of half-lap joints for both scales are shown in Figure 3.4.

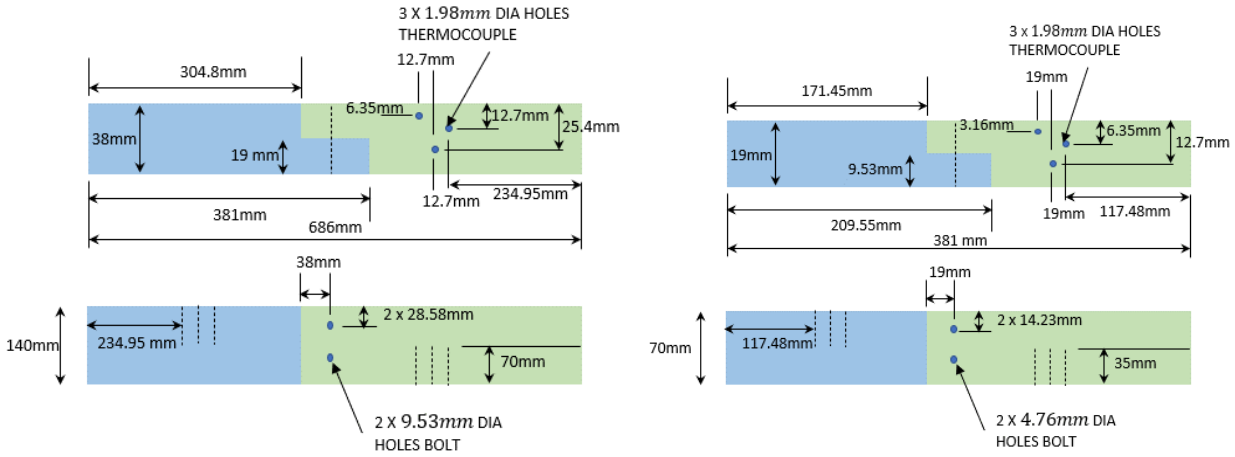

(a) (b)

Figure 3.4 Dimensions and drill locations of bolts and thermocouple holes in half-lap joint for (a) 1/2-scale (b) 1/4-scale

As seen in Figure 3.5 (a), the halves of each joint were glued individually, and samples were then clamped at the ends and along the length. The sample was then allowed to dry overnight. The halves were then drilled at locations shown in Figure 3.4 for thermocouple probes and bolts. These were then bolted as shown in Figure 3.5 (b) and (c). The moisture content of these wood half-lap joints was measured using a moisture meter to be 10.5%. General pin type Moisture meter with 0.1% accuracy was used. Finally, the edges of these test samples were painted with intumescent coating to prevent flames from rising from the edges to the unexposed side during the furnace tests. These samples were then allowed to condition for 48 hours prior to testing.

(a) (b) (c) (d) (e)

Figure 3.5 Preparation of half-lap joint (a) Each half of joint glued separately. Glued halves of half-lap joint bolted for (b) 1/4 scale (c) 1/2 scale. Edges of half-lap joint painted with intumescent coating for (d) 1/2 scale (e) 1/4 scale

3.2.1.3 Instrumentation

Furnace gas temperature was recorded using five Inconel-sheathed 1.5 mm diameter Type K thermocouple probes similar to Section 2.2.2 instrumentation. The average temperature was manually controlled by adjusting the gas flow rate in the burners using an Alicat MC-100 mass flow controller through a LabView interface, which also recorded the propane mass flow rate. The mass flow controller enabled the propane flow to be modified as necessary to maintain the desired furnace gas temperature during the test.

The thermal response was quantified through temperature measurements. These measurements were recorded at the center of each sample, 70 mm from the longer sides, and at two redundant locations 241mm from the short side ends, to disregard the edge effects like previous tests in Section 2.2.2. Consequently, there were two sets of temperature data for each sample. 76 mm thick sample had five probes at each of the two locations.

Omega high temp low drift thermocouple probes, Type K, grounded with a probe diameter of 1.57 mm were inserted to measure the depth temperatures. Two surface thermocouples were also attached to the bottom (unexposed side) for each of the test samples. Omega self-adhesive polyimide fast response Type K were used as surface thermocouples.

Two string potentiometers were used to measure the deflection of the half-lap joint which would be subjected to three-point bending. Celesco PT1DC-10-UP-Z10-MC4 potentiometers were used, and the range of potentiometers was 250 mm with an accuracy of 0.05% of full-scale. All gas temperatures, sample temperatures, and deflections were recorded using a LabView program at a frequency of 60 Hz.

3.2.1.4 Procedure

Six tests were carried out using the reduced scale furnace. The samples were subjected to fire exposure and static bending. The half-lap joints had been prepared at 686 mm and 381 mm lengths respectively for ½ and ¼ scales. However, these lengths included an overlap of 76 mm with the end supports for both scales. Therefore, the characteristic length L was 610 mm and 305 mm respectively as shown in Figure 3.6.

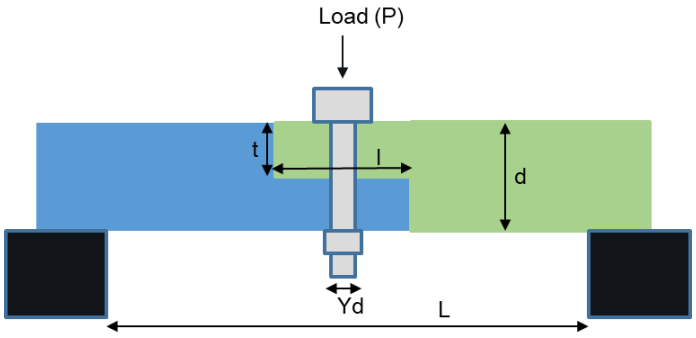

Figure 3.6 Characteristic length L in the half lap joint test

The test matrix as decided by the scaling methodology is shown in Table 3.1. For each test, samples were positioned on the furnace frame over the opening, exposing the central 610 mm. The furnace's remaining surface area not covered by the samples was obstructed with Type X gypsum wallboard barriers insulated with a 51 mm ceramic-fiber insulation blanket. To prevent flames from penetrating the sample's edge and ensuring heat transfer occurred solely through the sample's thickness, a ceramic-fiber insulation blanket was placed on the sides of the samples. Loads were

applied to the samples as per the test matrix. The initial deflection under the loading was measured before the furnace was turned on.

Two tests were conducted at ½ scale with the same load for repeatability. Next, for ¼ scale tests, the test setup end supports, and thermal barrier was modified as described above. For repeatability, two tests were conducted at the same load. Finally, wood boards at two scales were tested for comparison with half-lap joints.

Temperature at four depths and deflection were measured throughout for each of the test. The experiments were concluded after the samples failed visually under deflection or if the loads tilted out of the sample.

Upon completion of the exposure time, the gas supply to the furnace was shut off, the thermocouples were detached, and the sample was promptly taken out of the furnace to avoid additional exposure.

Table 3.1 Test matrix for half-lap joint subjected to thermo-structural furnace tests

Test	Scale (χ)	Type	Length L (mm)	Thickness 2t (mm)	Width (mm)	Load P (N)	Overlap l = 4t (mm)	Hole Yd (mm)
1	**Half (1/2)**	**Half-lap joint**	610	38	140	266.9	76	9.5
2			610	38	140	266.9	76	9.5
3	**Quarter (1/4)**		305	19	70	66.7	38	4.8
4			305	19	70	66.7	38	4.8
5	**Half (1/2)**	**Wood board**	610	38	140	266.9	--	--
6	**Quarter (1/4)**		305	19	70	66.7	--	--

3.3 Results

The objective of the furnace tests was to evaluate the performance of scaled joint assemblies and feasibility of scaling joints as seen in Section 3.2. First, we looked at the input furnace gas temperature curves for each test and compared them with the desired fire curves at each scale. The comparison is shown in Figure 3.7 where the average gas temperatures are calculated from the five thermocouples measuring the furnace. The actual fire curve temperatures matched well with the desired fire curve in the latter half of the tests, but initially deviated from the desired fire curves. We looked at the deviation errors by calculating the area under the curves for desired and actual. Area under the curves deviated 0.2 and 5% from desired in Tests 1 and 2, 10% and 11% from desired in Tests 3 and 4, and 8% and 9% in Tests 5 and 6. All the tests apart from tTst 4 were under the ASTM E119 defined limit of 10% error.

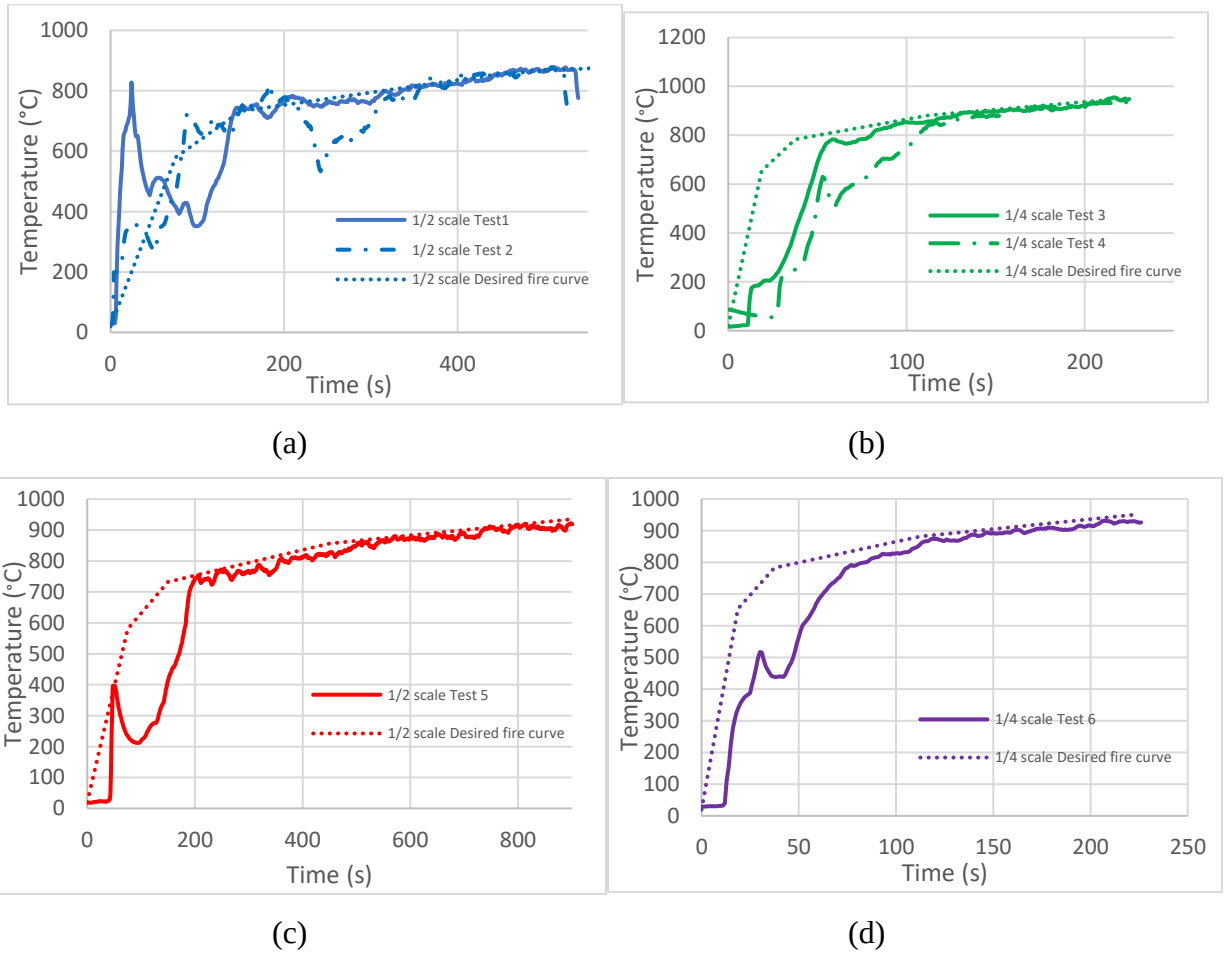

Figure 3.7 Desired vs actual furnace temperature comparison (a) Half-lap 1/2 scale (b) Half-lap joint 1/4 scale (c) Wood board 1/2 scale (d) Wood board 1/4 scale

After the tests, we looked at the failure. Visually, the ½ scale and ¼ scale half-lap joints failed identically as seen in Figure 3.8 (a). Both failed at the bolted overlap section by bearing shear at the bolts. Based on this, the failure of half-lap joints depends on diameter of the holes and their distance from the overlap edge. Failure in wood boards (no joints) was not at center but towards the right in both scales as seen in Figure 3.8 (b) but failures matched in wood boards at both scales. A possible reason for the off-center failure was test fixture asymmetry in terms of load placement.

(a) (b)

Figure 3.8 1/2 and 1/4 scale test samples after failure for (a) Half-lap joint (b) Wood board

The tests continued until failure as described in Section 3.2.1. In ASTM E119, the sample is defined to have failed if the maximum deflection reaches $\frac{L_c^2}{400d}$ and if the maximum deflection rate exceeds $\frac{L_c^2}{9000d}$ in 1 minute [1], where L_c is the characteristic length and d is the thickness of half-lap joint.

The deflections and rates corresponding to failure based on this definition were calculated and are summarized in Table 3.2.

Table 3.2 Failure as defined by ASTM E119 for half-lap joint and wood board

Parameters	Half-lap		Wood board	
	Half scale	Quarter scale	Half scale	Quarter scale
Lc (mm)	610	305	610	305
d (mm)	38	19	38	19
Max deflection (mm)	24	12	24	12
Max deflection rate (mm/min)	1.08	0.54	1.08	0.54

Deflections recorded were compared with the maximum and the times for failure for all tests were determined as shown in Table 3.3.

Table 3.3 Time for failure as defined by ASTM E119

Test	Type	Scale (χ)	Time for failure (s)	½ scale time : ¼ scale time
1	Half-lap joint	Half (1/2)	435	2.2:1
2			423	
3		Quarter (1/4)	198	
4			207	
5	Wood board	Half (1/2)	1532	3.03:1
6		Quarter (1/4)	505	

As seen in Section 3.1 scaling approach, the time was expected to scale as χ^2. Therefore, we had expected a time to failure ratio of 4:1 between ½ and ¼ scale. However, we obtained a 2.2:1 time scaling in half-lap joints and 3:1 time scaling in wood boards as seen in Table 3.3.

The temperature gradient was measured for each test at uniform depth as seen by the thermocouple locations described in Section 3.2.1. Average temperatures at each depth were calculated. If the temperature gradient versus time profiles for the ¼ and ½ scale test matched, a thermal similitude would be achieved between ½ and ¼ scales. To compare ½ and ¼ scale on the same plot we considered temperatures at effective time. ¼ scale effective time for half-scale tests was calculated by dividing each time step at which temperature was measured by 4 (considering 4:1 time scaling). Figure 3.9 (a) shows comparison between the ½ scale and ¼ scale temperature gradients with effective time for half-lap joint. We observed repeatability in temperature measurements between Tests 1 and 2, and Tests 3 and 4 respectively.

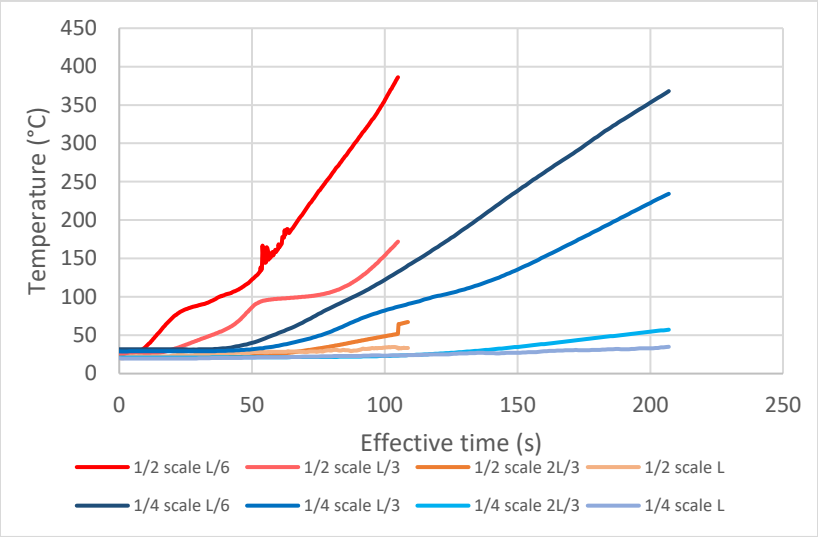

(a)

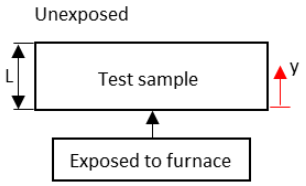

(b)

Figure 3.9 (a) Average temperature gradient comparison between 1/2 and 1/4 scale for half-lap joint (b) Depth coordinate location plotted at ¼ scale effective time

Similarly, deflections were also measured for each test at two locations. Average deflections were calculated. If the deflection versus time profiles for the ¼ and ½-scale test matched, a structural similitude would be achieved between ½ and ¼ scales. As in the temperature plot above, ¼ scale effective time for ½-scale tests was calculated by dividing each time step at which temperature was measured by 4 (considering 4:1 time scaling) to compare ½ and ¼ scale deflections on the same plot. Also, as seen in Section 3.1 scaling approach, we expected deflection to scale by χ. Therefore, to compare on same plot, we also divided ½ scale deflections by 2 (considering 2:1 deflection scaling) as shown in Figure 3.10. We observed repeatability in deflection measurements between Test 1 and 2, and Test 3 and 4 respectively.

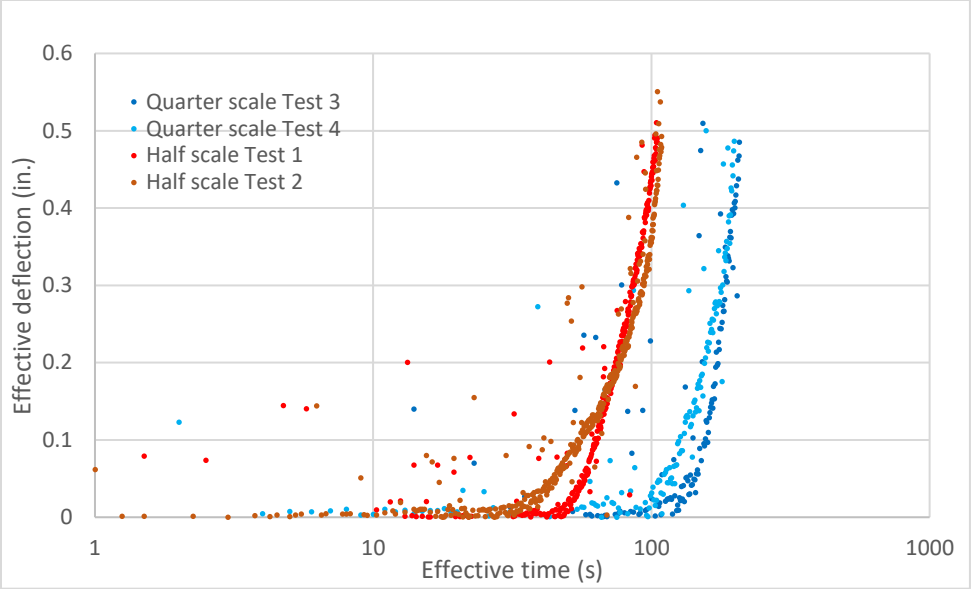

Figure 3.10 Effective deflection comparison between 1/2 and 1/4 scale for half-lap joint plotted at ¼ scale effective time

For thermo-structural similitude with Fourier time scaling, we should have seen an overlap of ½ and ¼ scale curves in Figure 3.9 (a) and Figure 3.10. However, for a 4:1 time scaling neither of the temperature and deflection plots matched between ½ and ¼ scale on effective time axis. As mentioned above, we observed 2.2:1 time scaling in half-lap joints. We investigated the reasons for this deviation in time scaling in the next section.

3.4 Discussion

3.4.1 Deviation in time scaling

In a previous study on wood boards subjected to thermo-structural tests Ref. [2], a 3.19:1 time scaling had been observed between ½ and ¼ scale tests instead of expected 4:1. The reason was that char formation did not scale the same as Fourier time scaling due to it being kinetically driven process. Charring rates and char conversion starting temperature both differed in ½ scale and ¼ scale. Thus, a char correction factor was calculated from the experimental data which corrected the time scaling between ½ and ¼ scale to 3.19:1. This was able to explain the failure time scaling (3:1) observed in wood board in our tests. However, this did not explain the additional deviation

(2.2:1 time scaling) in half-lap joints. Therefore, we investigated possible explanations for the additional deviation in time scaling.

These were the possible reasons explored:

1. Different failure modes in ½ and ¼ scale
2. Difference of transient heating in half-lap joints
3. Experimental error

3.4.1.1 Different failure modes in ½ and ¼ scale

According to ASTM E119, for a L/d = 24, bending stress completely dominates the effective stress [1], where L is the characteristic length, and d is thickness. In our tests, half-lap joints had a L/d = 16. There was a chance that shear stress would factor in the total stress. Therefore, we looked at the possible shear stresses on the joint. Subscripts 1 and 2 denote full scale and reduced scale dimensions respectively.

3.4.1.1.1 Shear stress across cross section (S)

S = Transverse force / cross section area

Shear force = P/2

Minimum cross section area = d(b-2Yd)

$$S = \frac{P/2}{(b-2Y_d)d} \tag{3.13}$$

$$Y_{d2} = \chi Y_{d1} \tag{3.14}$$

$$S_1 = \frac{P_1}{2(b_1-2Y_{d1})d_1} \tag{3.15}$$

$$S_2 = \frac{P_2}{2(b_2-2Y_{d2})d_2} \tag{3.16}$$

From (3.2), (3.3) and (3.8)

$$S_2 = \frac{\chi^2 P_1}{2(\chi b_1-2\chi Y_{d1})\chi d_1}$$

$$S_2 = S_1 \tag{3.17}$$

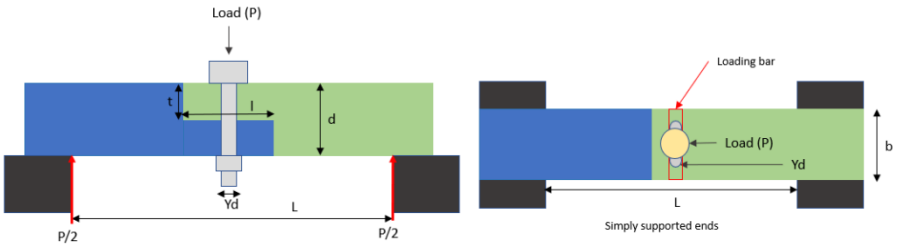

(a) (b)

Figure 3.11 Shear stress due to load P (a) Front view (b) Top view

3.4.1.1.2 Horizontal shear stress (S_h)

$$\text{Shear flow } q = \frac{VQ}{I} = \frac{F}{l} \tag{3.18}$$

where, V the shear force perpendicular to neutral axis, Q is the first moment of area about the neutral axis above the depth, I is the second moment of area, F is the shear force parallel to neutral axis and l is the overlap length.

$$Q = \frac{1}{2}\left(\frac{d}{2}\right)\left(b\frac{d}{2}\right) \tag{3.19}$$

$$Q = \frac{bd^2}{8} \tag{3.20}$$

$$I = \frac{bd^3}{12} \tag{3.21}$$

From (3.18), (3.19) and (3.20),

$$q = \frac{\left(\frac{P}{2}\right)\left(\frac{bd^2}{8}\right)}{\frac{bd^3}{12}} = \frac{F}{l}$$

$$F = \frac{3}{4}\frac{Pl}{d} \tag{3.22}$$

$$\text{Cross section area } A_h = l(b\text{-}2Y_d) \tag{3.23}$$

$$S_h = \frac{F}{A_h} \tag{3.24}$$

$$S_h = \frac{3}{4}\frac{P}{d(b-2Y_d)} \tag{3.25}$$

$$S_{h1} = \frac{3}{4}\frac{P_1}{d_1(b_1-2Y_{d1})} \tag{3.26}$$

$$S_{h2} = \frac{3}{4}\frac{P_2}{d_2(b_2-2Y_{d2})} \tag{3.27}$$

From (3.2), (3.3) and (3.8),

$$S_{h2} = \frac{3}{4}\frac{\chi^2 P_1}{\chi d_1 \chi (b_1 - 2Y_{d1})}$$

$$S_{h1}=S_{h2} \tag{3.28}$$

We had seen that the bending stress was equal across scales in Section 3.1. Therefore, as the bending as well as shear stresses were equal between the two scales, the total stress would also be equal between them. Therefore, this was ruled out as a reason for time scaling deviation.

3.4.1.2 Difference of transient heating in half-lap joints

In our scaling approach we had assumed a 1-D heat transfer through the half-lap joint thickness to be sufficient for scaling. However, there was a possibility that the heat transfer through the bolts due to bolt radius effect did not follow Fourier time scaling of 4:1. Also, due to higher thermal conductivity of steel bolts compared to wood, there was a possibility that heat conduction through the bolt was non-negligible and hence affected the overall time scaling. Therefore, we looked at heat transfer through bolts due to transient heat conduction to investigate the effect of bolt radius and bolt length on time scaling.

For 2-D heat transfer through the bolt,

$$\frac{\partial T}{\partial t} = \alpha\left(\frac{\partial^2 T}{\partial x^2}\right) + \left(\frac{1}{\rho C}\right)\left[\frac{1}{r}\frac{\partial}{\partial r}\left(rk\frac{\partial T}{\partial r}\right)\right] \tag{3.29}$$

where, α is thermal diffusivity, ρ is density, C is specific heat and k is thermal conductivity.

$$\frac{\partial T}{\partial t} = \alpha\left(\frac{\partial^2 T}{\partial x^2}\right) + \left(\frac{k}{\rho C}\right)\left[\frac{1}{r}\frac{\partial}{\partial r}\left(r\frac{\partial T}{\partial r}\right)\right]$$

$$\frac{\partial T}{\partial t} = \alpha\left(\frac{\partial^2 T}{\partial x^2}\right) + \alpha\left[\frac{1}{r}\left(\frac{\partial T}{\partial r} + r\frac{\partial^2 T}{\partial r^2}\right)\right]$$

$$\frac{\partial T}{\partial t} = \alpha\left(\frac{\partial^2 T}{\partial x^2}\right) + \alpha\left(\frac{\partial^2 T}{\partial r^2}\right) + \frac{\alpha}{r}\left(\frac{\partial T}{\partial r}\right) \tag{3.30}$$

Nondimensionalize using,

$$T' = \frac{T}{T_f^{max}} \tag{3.31}$$

$$t' = \frac{t}{\tau} \tag{3.32}$$

$$x' = \frac{x}{L} \tag{3.33}$$

$$r' = \frac{r}{D} \tag{3.34}$$

where, T_f^{max} is maximum furnace temperature, L is bolt length, and D is bolt diameter.

$$\frac{\partial T'}{\partial t'} = \frac{\alpha\tau}{L^2}\left(\frac{\partial^2 T'}{\partial x'^2}\right) + \frac{\alpha\tau}{D^2}\left(\frac{\partial^2 T'}{\partial r'^2}\right) + \frac{\alpha\tau}{D^2 r'}\left(\frac{\partial T'}{\partial r'}\right) \tag{3.35}$$

From this, we identified the non-dimensional groups

$$\frac{\alpha\tau}{L^2} \tag{3.36}$$

$$\frac{\alpha\tau}{D^2} \tag{3.37}$$

$$\frac{\alpha\tau}{D^2} \tag{3.38}$$

From the Equations (3.36), (3.37) and (3.38), for $L_2=\chi L_1$ and $D_2=\chi D_1$,

$\tau_2 = \chi^2 \tau_1$

Therefore, time should scale as χ^2. We confirmed this by simulating transient heat conduction in Ansys Mechanical. First, we created a 3-D model of half-lap joint at ½ and ¼ scales. Boundary conditions on the unexposed side with a heat transfer coefficient of 4 W/m^{2}K [45], emissivity 0.8 [46], and ambient temperature of 20°C. Boundary conditions on the exposed side were heat transfer coefficient of 25 W/m^{2}K, emissivity of 0.8, and the furnace gas temperatures. The furnace temperatures were input as desired half scale temperatures for ½ scale model and for ½ scale model, at three different time scales 2:1, 3:1 and 4:1. Simulation results shown in Figure 3.12 (a) to (d) show that 3:1 and 2:1 time scaling leads to higher temperatures in ¼ scale compared to ½ scale, as was expected. To quantify the temperatures, a plot of temperatures along the white line which connects the ends of the overlap region in Figure 3.12 (e) and (f) show that a 4:1 time scaling was correct for thermal similitude. Thus, our assumption of Fourier time scaling was correct.

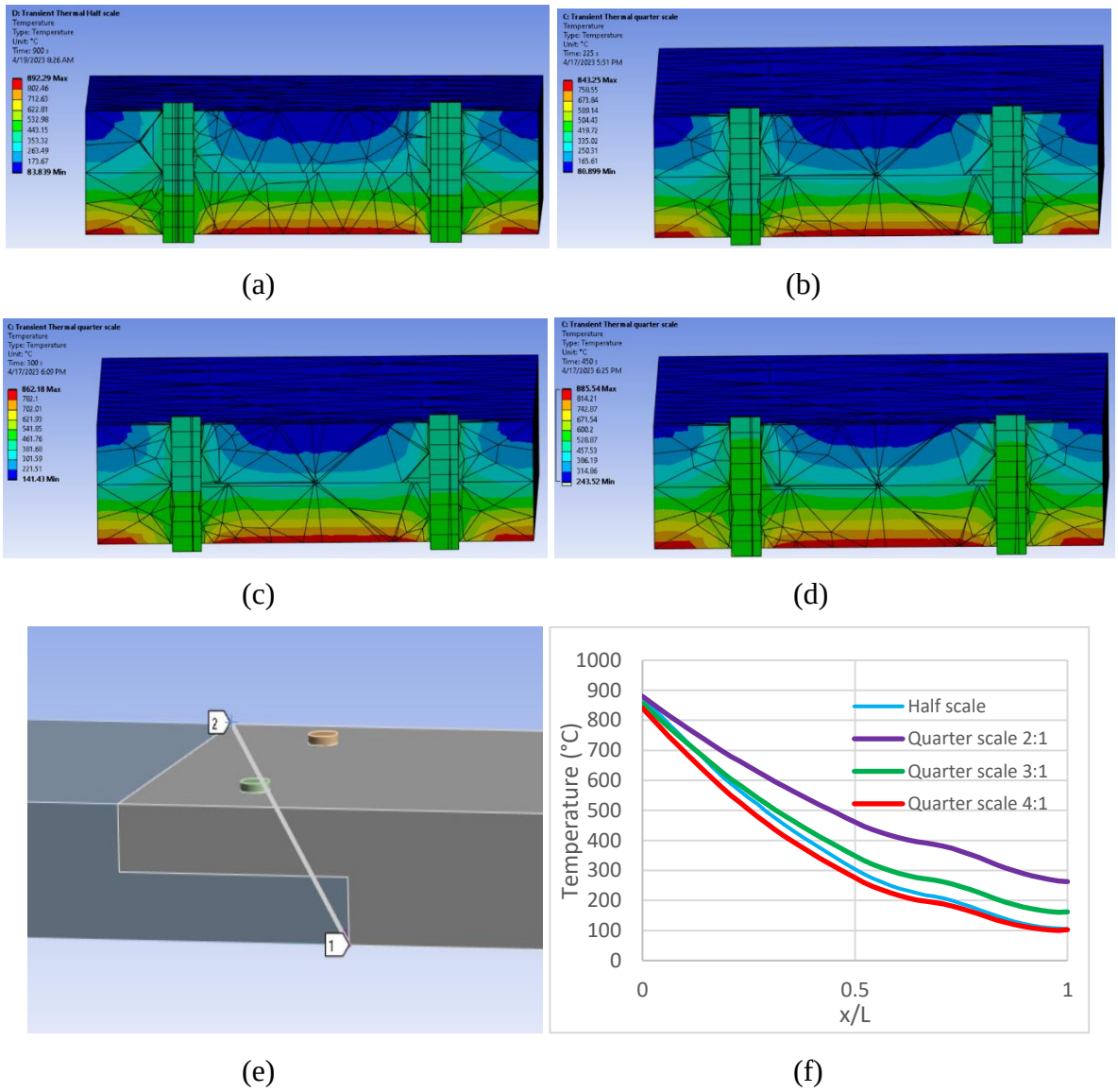

Figure 3.12 Temperature comparison for different time scaling (a) ½ scale model (b) 4:1 ¼ scale (c) 3:1 ¼ scale (d) 2:1 ¼ scale (e) Location of temperature probe (f) Temperatures along white line

3.4.1.3 Experimental error

Once we had confirmed that the physics behind the scaling was correct, we looked at errors in the experiment. While individually, the furnace temperatures were within the limits as seen in Section 3.3, we also compared the actual and desired curves at both scales together, because while ½ scale temperature area under curve was close to the desired (less than 5%), ¼ scale deviated the most (11%). Once again, the comparison was made at half-scale effective time, and is shown in Figure 3.13.

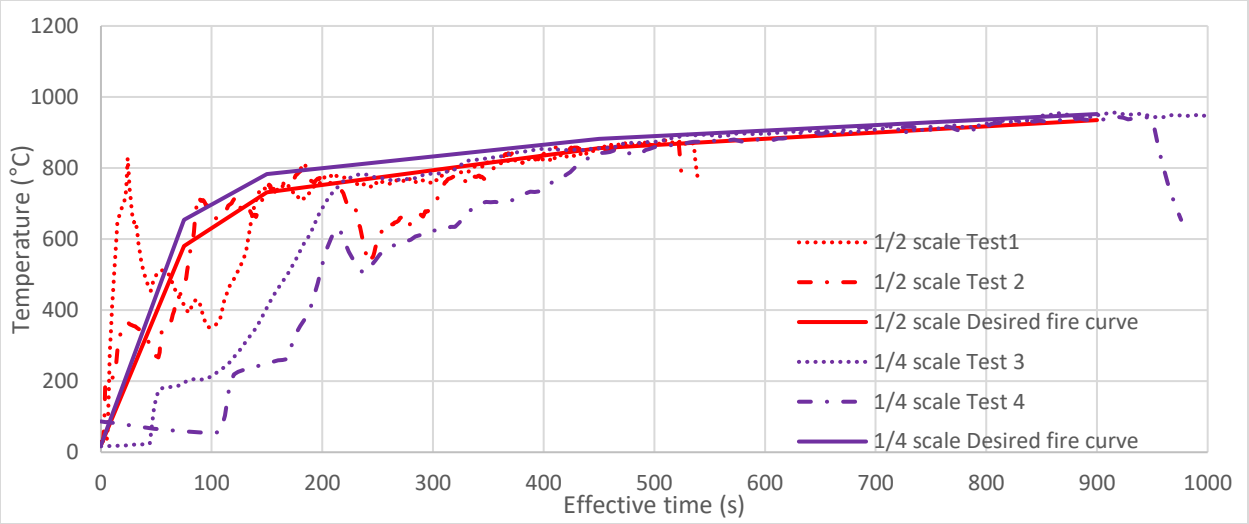

Figure 3.13 Comparison of desired and actual furnace temperatures for 1/2 vs 1/4 scale plotted at ½ scale effective time

From the plot, the desired ¼ scale fire curve is at a higher temperature compared to ½ scale fire curve. This is so that heat flux is maintained at the furnace exposed side of the half-lap joint. However, actual ¼ scale fire curves were significantly lower than ½ scale fire curves until an effective time of 300 seconds. This meant that it would take a lot longer for the ¼ scale test samples to reach the same temperatures as that of ½ scale test samples which would explain time scaling extending from 4:1 to 2.2:1. Our belief was that the additional deviation was a result of the furnace temperature. The reason for the additional time scaling difference was caused by inaccurate control of the gas temperature during the ¼ scale tests. To confirm this, we again simulated transient heat conduction in Ansys Mechanical. However, instead of ideal furnace gas temperatures, used the actual input furnace temperatures in ½ and ¼ scale models. Therefore, the ½ scale model was heated for 435s, and the ¼ scale model was heated for 198s. Figure 3.14 (b) shows the temperatures along the white line shown in (a) which was at the center of the overlap at length and depth and measured temperatures along the width at the end of their respective tests. Temperatures matched between ½ and ¼ scales with an applied time ratio of 2.2:1 in Ansys. This was in line with what was observed experimentally.

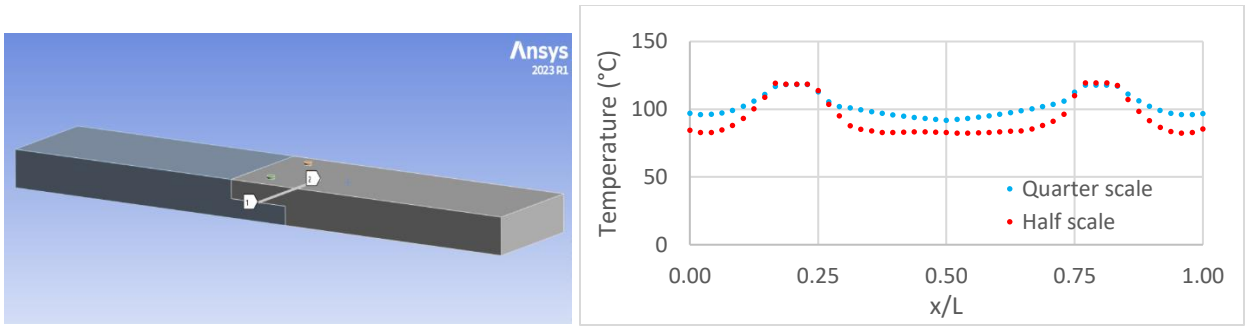

(a) **(b)**

Figure 3.14 (a) Location of temperature probe at center of half-lap joint depth and length(b) Temperature comparison for actual furnace gas input temperatures along probe

3.4.2 Scaling in half-lap joint

Once we had explained the deviation in time scaling, we compared the temperature gradients again with corrected time scaling. For comparison, temperatures at four depths were plotted against effective time which was calculated by considering 2.2:1 time ratio shown in Figure 3.15 (a). Average temperatures were calculated using two test measurements except at depth L/6 and L/3 in ½ scale, where erratic measurements had been observed in Test 2 and only Test 1 temperatures were plotted. If we observed an overlap between ½ scale and ¼ scale temperatures at all depths along effective time, it would mean that the ½ and ¼ scale were in thermal similitude for corrected time scaling including the experimental error in the exposure.

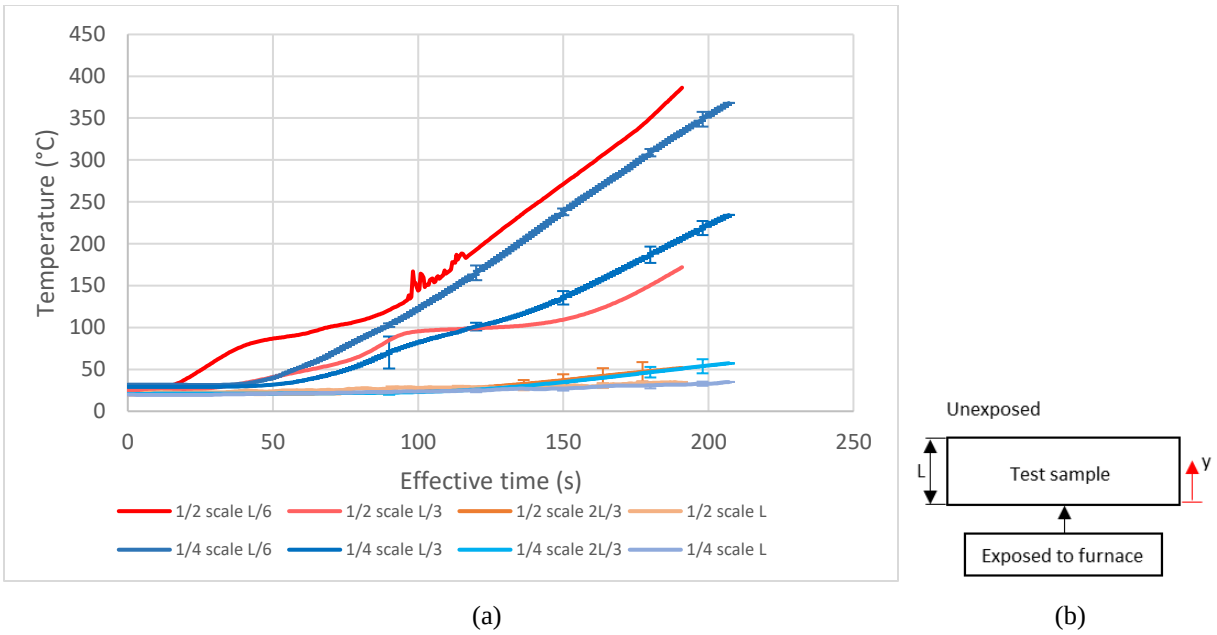

(a) (b)

Figure 3.15 (a) Temperature gradient comparison between 1/2 and 1/4 scale for half-lap joint with corrected time scaling and error bars plotted at ¼ scale effective time (b) Depth coordinate location

From the plot, we observed a good match between ½ and ¼ scale temperatures at all depths, and there was a close overlap between both temperature and time between the two scales. The error increased with temperature measurements close to the furnace exposed side, while the error was negligible at the unexposed side. We plotted the temperatures at failure along four depths to analyze these errors quantitatively.

The failure time of Test 2 was considered because it was the smallest failure time among Tests 1 through 4. Test 1 temperatures at that same time were used and for ¼ scale tests the failure time was converted to ½ scale effective time by using a 2.2:1 time scaling ratio to include exposure experimental error. The temperatures corresponding to this effective time were taken from Tests 3 and 4. Temperature measurements had been recorded along four depths at two locations for each test. Temperatures at depths L/6 and L/3 from the side exposed to furnace were erratic throughout test 2 due to faulty thermocouple probes and were excluded from the analysis. Depth ratio y/L = 0 corresponds to the furnace exposed side and y/L = 1 to the unexposed side. The plot is shown in Figure 3.16.

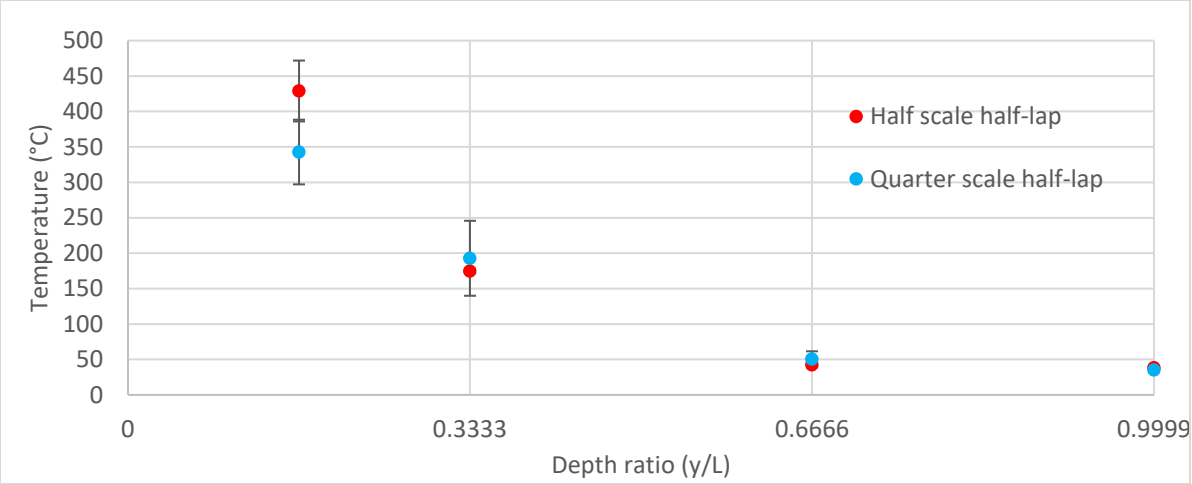

Figure 3.16 Temperature gradient in half-lap joint at ½ scale effective failure time with error bars

The relative errors at each depth were tabulated as shown in Table 3.4. As seen visually, the relative errors increased as we moved towards the furnace exposed side. Overall, there was a good match between the ½ and ¼ scale temperatures with the highest relative error of 20%. The lowest relative error was 8.8% at the unexposed side. Depth of L/6 (depth ratio 0.167) had the highest uncertainty in measurements. ¼ scale measurements had the higher uncertainty of the two scales.

Table 3.4 Relative error between 1/2 and 1/4 scale temperature gradient in half-lap joint

Depth ratio	Half-scale temperatures (°C)	Quarter-scale temperatures (°C)	% Relative Error
0.167	429 ± 32.5	343 ± 46	20.1
0.33	175 ± 3	193 ± 53	10.2
0.67	42 ± 3	51 ± 11	19.1
1	38 ± 3	35 ± 3	8.8

Thus, we can conclude that

1. The overlap of temperature versus time between ½-scale and ¼-scale was satisfactory.
2. Thermal similitude was achieved between the two scales with a time scale ratio of 2.2:1, which includes the experimental error in the exposure. If the exposures were closer to the theoretical levels, a time scale ratio of approximately 3:1 would be expected similar to that achieved in the wood board tests.

Deflection measurements were recorded at two locations in each test. Now, we compared the deflections by calculating the average for two tests with two measurements in each test, with the

corrected time scaling. ¼ scale effective deflections were plotted against ¼ scale effective time (see in Figure 3.17) which was calculated by considering 2.2:1 time scaling ratio to include exposure error. Again, as seen in Section 3.1 scaling approach, we expected deflection to scale by χ. Therefore, to compare on same plot, the ¼ scale effective deflection for the ½ scale tests was determined by dividing the half-scale deflections by 2. If we observed an overlap between ½ scale and ¼ scale effective deflections along effective time, it would mean that the ½ and ¼ scale were in structural similitude for corrected time scaling.

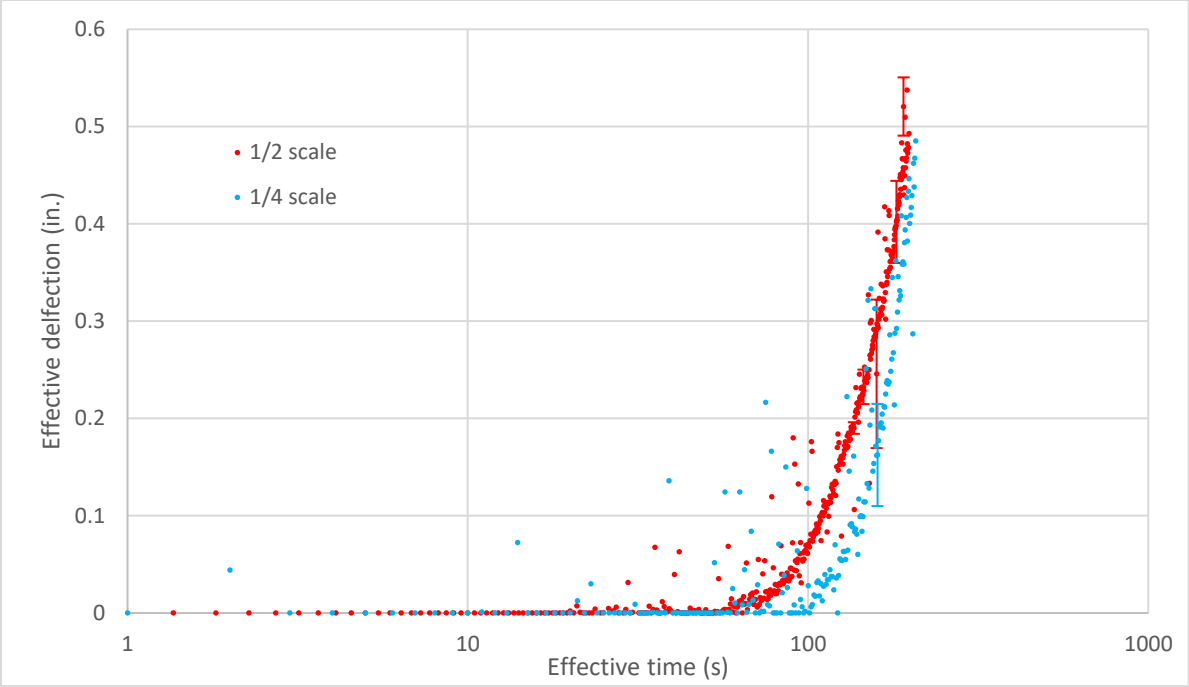

Figure 3.17 Effective ¼ scale deflection comparison between 1/2 and 1/4 scale for half-lap joint with corrected time scaling and error bars plotted at ¼ scale effective time

There was a lot of noise observed in deflection measurements during the initial test period. The overlap between the two scales was less during the initial phase implying higher error; however, the two scales overlapped towards the failure with a low error. Overall, a good match was observed between ½ and ¼ scale deflections with time with low errors. We plotted the effective deflections at different times to better quantify these errors.

Failure time of Test 2 was considered because it was the smallest failure time among Tests 1 through 4. ¼ scale effective deflections were plotted at ¼ scale effective time (considering 2.2:1 time scaling) 48, 95, 143, 162, 191s.

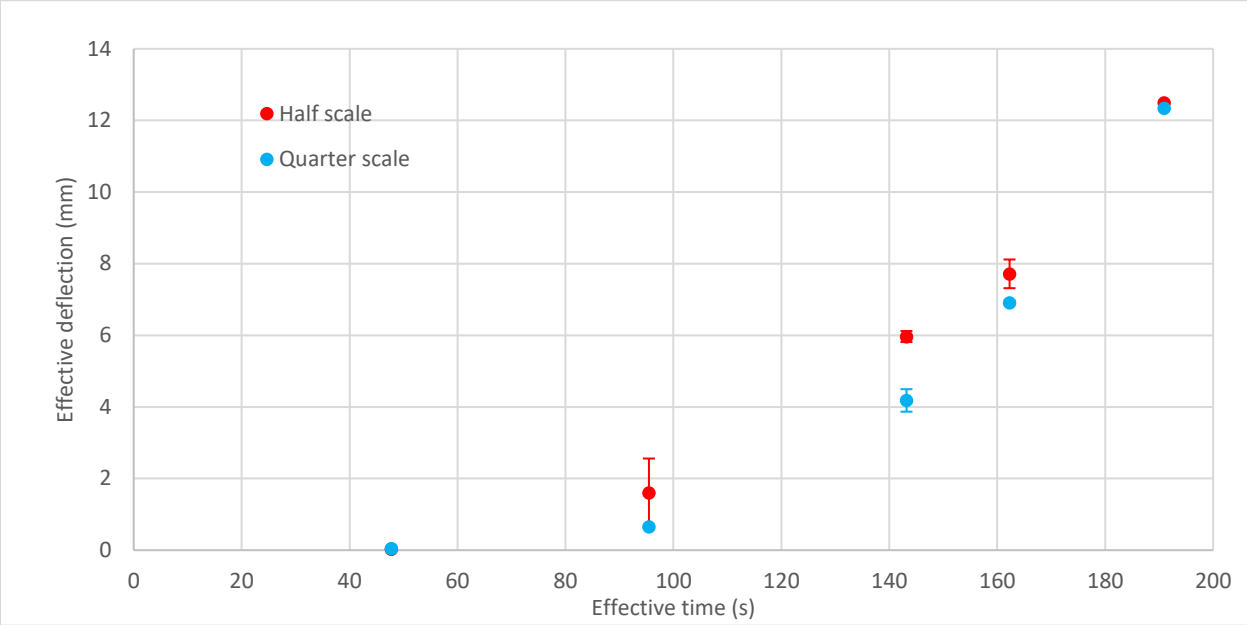

Figure 3.18 ¼ scale effective deflection comparison between 1/2 and 1/4 scale half-lap joints with error bars plotted at ¼ scale effective time

The relative deflection errors were tabulated as shown in Table 3.5. The highest error was observed at 48s but since the samples hadn't started to deflect this was of no importance. From 95s the deflections were noticeable, and there was initially a high relative error of 59% between the ½ and ¼ scale deflections. As seen in the plot in Figure 3.18, the relative errors decreased as the joint moved towards failure. The relative error was less than 10% in the latter stages close to failure and 1% at failure. Good repeatability was observed between Tests 1 and 2, and Tests 3 and 4 respectively seen by low uncertainties in measurement. Uncertainties were calculated from the average deflections measured in two tests for both scales each.

Table 3.5 Relative error between 1/2 and 1/4 scale effective deflection in half-lap joint

Effective time (s)	Effective deflection in half-lap joint (mm)				Combined uncertainty	% Relative error
	Half scale		Quarter scale			
48	0.03	± 0.003	0.05	± 0.013	0.013	89
95	1.61	± 0.095	0.66	± 0.045	0.954	59
143	5.97	± 0.154	4.18	± 0.314	0.350	30
162	7.72	± 0.401	6.91	± 0.50	0.404	10
191	12.49	± 0.029	12.34	± 0.016	0.033	1

The scaling of half-lap joint did not work as had been expected. However, this was due to an experimental input error, in supplying correct furnace gas temperatures at ¼ scale tests and char correction. This error caused the time to scale by 2.2:1 instead of the expected 4:1 to maintain thermo-structural similitude. However, with this correction in time scaling, we observed that the deflections did scale and the temperature gradients did match between the ½ and ¼ scale half-lap joint.

This indicates that with a better furnace input control, we should be able to scale ASTM E119 test for half-lap joints to maintain thermo-structural similitude with a time-scaling of closer to 3.2:1 to account for the char formation kinetics.

3.5 Summary

A methodology used to scale ASTM E119 fire resistance test for dimensional lumber was updated to cover wood based half-lap joints. The developed methodology was tested on half-lap joints which were subjected to thermal and structural loading in the furnace in our lab. Three-point bending tests were performed on half-lap joints at ½ and ¼ scale. Thermo-structural similitude was observed between ½ and ¼ scale when time was scaled by a factor 2.2:1 (due to combination of exposure experimental error at ¼ scale and char correction). With more accurate control of gas temperature at ¼ scale, the time scaling similar to that found for wood boards (no joints), which is approximately 3.2:1 since the char formation kinetics do not scale.

Chapter 4 Conclusions and future work

4.1 Conclusions

In this thesis, a methodology which was previously used on dimensional lumber in a past study was updated to cover different types of wood-based structures to reduce their sizes while successfully maintaining a thermo-structural similitude between the original scale and the reduced scale. The second chapter investigated scaling fire resistant coated wood under fire exposure and evaluated the extent to which the scaling was successful. The third chapter investigated the feasibility of scaling joints and the performance of the scaled joints under thermal and structural loading. The following conclusions were derived:

1. A methodology was developed to scale fire resistant coated wood. This developed methodology was tested on a commercially available intumescent coating. The methodology successfully worked for scaling intumescent coating-wood assembly from full to ½ scale while maintaining the same thermal response.
2. This did not however scale down to ¼ scale. Very low dry film thickness of the intumescent coating for the ¼ scale test coupled with short test time of 225s meant that the intumescent coating could not expand to its maximum thickness. Result indicates that the ¼ scale and ½ scale DFT should be the same. Further study must be done to improve the expansion correlation between dry film thickness (DFT) and final thickness for low DFTs and very small test times.
3. The importance of developing a methodology was that the same scaling might not work for other types of coatings, even other intumescent coatings might need a different scaling. This scaling methodology can be used to develop a scaling relationship for other types of coatings.
4. A methodology used to scale ASTM E119 fire resistance test for dimensional lumber was updated to cover wood based half-lap joints. This included scaling the dimensions of the sample, joint, and bolts. Thermo-structural similitude was observed between ½ and ¼ scale when time was scaled by a factor 2.2:1. A combination of gas temperature exposure error in the ¼ scale tests and char formation kinetics were found to be responsible for the deviation in time scaling from the theoretical value of 4:1 to 2.2:1. Better control of the

exposure gas temperature would result in half-lap joint scaling to be more similar to that of wood boards (no joints), which have a ¼ to ½ time scaling of approximately 3.2:1. This is less than the theoretical 4:1 ratio due to char formation kinetics.

5. The failure time of half-lap joints depends on diameter of the holes and their distance from the overlap edge due to shear stress acting on wood. The diameter of the bolts had a big impact on the scaling of the thermal response. Bolt geometry should be scaled linearly with the wood substrate to maintain thermal similitude.

4.2 Future work

4.2.1 Scaling fire-resistant coated wood for thermal only test

The scaling methodology worked for scaling size of intumescent coating-wood assembly from full to ½ scale only. Further study must be done to improve the expansion correlation between dry film thickness (DFT) and final thickness for low DFTs and very small test times for successfully scaling intumescent coating-wood assembly from full to ¼ scale.

The developed scaling methodology was tested for one commercially available intumescent coating. In future it should be tested on other available intumescent coatings to validate the success of scaling intumescent coating-wood assembly for fire exposure tests.

Also, while the scaling methodology was tested on intumescent coatings, there are other types of fire-resistant coatings like MgO based coatings, which don't expand with fire exposure. These should be tested using the developed scaling methodology to validate successful scaling for fire-resistant coated wood. There might be some additional steps required while testing other types of coatings, depending on the availability and ease of varying coating thicknesses.

Finally, in this study, only the thermal response of fire-resistant coated wood was scaled. In future work, the feasibility of scaling its thermo-structural response should be investigated.

4.2.2 Scaling wood-based joints for thermo-structural test

In this study, the developed scaling approach was tested on half-lap joints. There are other types of joints used in structural assemblies which are tested by ASTM E119. This scaling approach should be tested on these other joints.

The failure time of half-lap joints depends on diameter of the holes and their distance from the overlap edge. Further study is required on testing the effects of bolts on the failure time. Bolt diameters, numbers, pattern, etc. should be investigated. Currently the spacing between the bolts was fixed by considering the minimum distance requirement of 1.5d from the edges and symmetry along the overlap region, where d is the diameter of bolt. Future works should investigate the individual and combined effects of all these parameters on fire resistance.

References

[1] ASTM E119, "Standard Test Methods for Fire Tests of Building Construction and Materials," *ASTM International*, vol. 552. ASTM, pp. 1–36, 2008.

[2] M. J. Gangi *et al.*, "Scale Modeling of Tests with Combined Thermo-Structural Loading," 2023.

[3] R. G. Puri and A. S. Khanna, "Intumescent coatings: A review on recent progress," *J Coat Technol Res*, vol. 14, no. 1, pp. 1–20, Jan. 2017, doi: 10.1007/s11998-016-9815-3.

[4] M. A. Hassan, R. Kozlowski, and B. Obidzinski, "New fire-protective intumescent coatings for wood," *J Appl Polym Sci*, vol. 110, no. 1, pp. 83–90, Oct. 2008, doi: 10.1002/app.28518.

[5] A. Lucherini, Q. S. Razzaque, and C. Maluk, "Exploring the fire behaviour of thin intumescent coatings used on timber," *Fire Saf J*, vol. 109, Oct. 2019, doi: 10.1016/j.firesaf.2019.102887.

[6] A. Hussain, V. Landry, P. Blanchet, D.-T. Hoang, and C. Dagenais, "Fire Performance of Intumescent Waterborne Coatings with Encapsulated APP for Wood Constructions," 2021, doi: 10.3390/coatings.

[7] J. E. J. Staggs, R. J. Crewe, and R. Butler, "A theoretical and experimental investigation of intumescent behaviour in protective coatings for structural steel," *Chem Eng Sci*, vol. 71, pp. 239–251, Mar. 2012, doi: 10.1016/j.ces.2011.12.010.

[8] G. Q. Li, C. Zhang, G. B. Lou, Y. C. Wang, and L. L. Wang, "Assess the Fire Resistance of Intumescent Coatings by Equivalent Constant Thermal Resistance," *Fire Technol*, vol. 48, no. 2, pp. 529–546, Apr. 2012, doi: 10.1007/s10694-011-0243-8.

[9] H. C. Chang, W. H. Park, K. B. Yoon, T. K. Kim, D. H. Lee, and W. S. Jung, "Inverse estimation of properties for charring material using a hybrid genetic algorithm," *Journal of Mechanical Science and Technology*, vol. 25, no. 6, pp. 1429–1437, Jun. 2011, doi: 10.1007/s12206-011-0402-3.

[10] R. J. Asaro, B. Lattimer, C. Mealy, and G. Steele, "Thermo-physical performance of a fire protective coating for naval ship structures," *Compos Part A Appl Sci Manuf*, vol. 40, no. 1, pp. 11–18, Jan. 2009, doi: 10.1016/j.compositesa.2008.07.015.

[11] E. Kandare, G. J. Griffin, S. Feih, A. G. Gibson, B. Y. Lattimer, and A. P. Mouritz, "Fire structural modelling of fibre-polymer laminates protected with an intumescent coating,"

Compos Part A Appl Sci Manuf, vol. 43, no. 5, pp. 793–802, May 2012, doi: 10.1016/j.compositesa.2011.05.012.

[12] B. K. Cirpici, Y. C. Wang, and B. Rogers, "Assessment of the thermal conductivity of intumescent coatings in fire," *Fire Saf J*, vol. 81, pp. 74–84, Apr. 2016, doi: 10.1016/j.firesaf.2016.01.011.

[13] A. Lucherini and C. Maluk, "Intumescent coatings used for the fire-safe design of steel structures: A review," *Journal of Constructional Steel Research*, vol. 162. Elsevier Ltd, Nov. 01, 2019. doi: 10.1016/j.jcsr.2019.105712.

[14] A. Lucherini and C. Maluk, "Assessing the onset of swelling for thin intumescent coatings under a range of heating conditions," *Fire Saf J*, vol. 106, pp. 1–12, Jun. 2019, doi: 10.1016/j.firesaf.2019.03.014.

[15] Y. Zhang, Y. C. Wang, C. G. Bailey, and A. P. Taylor, "Global modelling of fire protection performance of intumescent coating under different cone calorimeter heating conditions," *Fire Saf J*, vol. 50, pp. 51–62, May 2012, doi: 10.1016/j.firesaf.2012.02.004.

[16] Z. Han, A. Fina, G. Malucelli, and G. Camino, "Testing fire protective properties of intumescent coatings by in-line temperature measurements on a cone calorimeter," *Prog Org Coat*, vol. 69, no. 4, pp. 475–480, Dec. 2010, doi: 10.1016/j.porgcoat.2010.09.001.

[17] L. Wang, Y. Dong, C. Zhang, and D. Zhang, "Experimental Study of Heat Transfer in Intumescent Coatings Exposed to Non-Standard Furnace Curves," *Fire Technol*, vol. 51, no. 3, pp. 627–643, May 2015, doi: 10.1007/s10694-015-0460-7.

[18] A. Elliott, A. Temple, C. Maluk, and L. Bisby, "Novel Testing to Study the Performance of Intumescent Coatings under Non-Standard Heating Regimes," *Fire Safety Science*, vol. 11, pp. 652–665, 2014, doi: 10.3801/IAFSS.FSS.11-652.

[19] A. Lucherini, L. Giuliani, and G. Jomaas, "Experimental study of the performance of intumescent coatings exposed to standard and non-standard fire conditions," *Fire Saf J*, vol. 95, pp. 42–50, Jan. 2018, doi: 10.1016/j.firesaf.2017.10.004.

[20] M. Bartholmai, R. Schriever, and B. Schartel, "Influence of external heat flux and coating thickness on the thermal insulation properties of two different intumescent coatings using cone calorimeter and numerical analysis," *Fire Mater*, vol. 27, no. 4, pp. 151–162, Jul. 2003, doi: 10.1002/fam.823.

[21] T. Fateh, E. Guillaume, and P. Joseph, “An experimental study of the thermal performance of a novel intumescent fire protection coating,” *Fire Saf J*, vol. 92, pp. 132–141, Sep. 2017, doi: 10.1016/j.firesaf.2017.05.021.

[22] M. Wilson, B. Dlugogorski, and E. Kennedy, “Uniformity Of Radiant Heat Fluxes In Cone Calorimeter,” *Fire Safety Science*, vol. 7, pp. 815–826, 2003, doi: 10.3801/IAFSS.FSS.7-815.

[23] B. Schartel, M. Bartholmai, and U. Knoll, “Some comments on the use of cone calorimeter data,” *Polym Degrad Stab*, vol. 88, no. 3, pp. 540–547, Jun. 2005, doi: 10.1016/j.polymdegradstab.2004.12.016.

[24] B. Gardelle, S. Duquesne, V. Rerat, and S. Bourbigot, “Thermal degradation and fire performance of intumescent silicone-based coatings,” *Polym Adv Technol*, vol. 24, no. 1, pp. 62–69, Jan. 2013, doi: 10.1002/pat.3050.

[25] M. Muller *et al.*, “Investigation of the synergy in intumescent polyurethane by 3D computed tomography,” *Polym Degrad Stab*, vol. 98, no. 9, pp. 1638–1647, Sep. 2013, doi: 10.1016/j.polymdegradstab.2013.06.018.

[26] L. L. Wang, Y. C. Wang, J. F. Yuan, and G. Q. Li, “Thermal conductivity of intumescent coating char after accelerated aging,” *Fire Mater*, vol. 37, no. 6, pp. 440–456, Oct. 2013, doi: 10.1002/fam.2137.

[27] M. Jimenez, S. Duquesne, and S. Bourbigot, “Multiscale experimental approach for developing high-performance intumescent coatings,” *Ind Eng Chem Res*, vol. 45, no. 13, pp. 4500–4508, Jun. 2006, doi: 10.1021/ie060040x.

[28] L. Calabrese, F. Bozzoli, G. Bochicchio, B. Tessadri, S. Rainieri, and G. Pagliarini, “Thermal characterization of intumescent fire retardant paints,” in *Journal of Physics: Conference Series*, Institute of Physics Publishing, 2014. doi: 10.1088/1742-6596/547/1/012005.

[29] R. ; Fahrni *et al.*, “SiF,” 2018, doi: 10.3929/ethz-b-000269112.

[30] D. de Silva, A. Bilotta, and E. Nigro, “Experimental investigation on steel elements protected with intumescent coating,” *Constr Build Mater*, vol. 205, pp. 232–244, Apr. 2019, doi: 10.1016/j.conbuildmat.2019.01.223.

[31] Y. Zhang, Y. C. Wang, C. G. Bailey, and A. P. Taylor, “Global modelling of fire protection performance of an intumescent coating under different furnace fire conditions,” *J Fire Sci*, vol. 31, no. 1, pp. 51–72, Jan. 2013, doi: 10.1177/0734904112453566.

[32] C. Maraveas, K. Miamis, and C. E. Matthaiou, “Performance of Timber Connections Exposed to Fire: A Review,” *Fire Technol*, vol. 51, no. 6, pp. 1401–1432, Nov. 2015, doi: 10.1007/s10694-013-0369-y.

[33] C. Austruy, M. Fragiacomo, P. Moss, and A. Buchanan, “Fire resistance of timber connections,” 2007.

[34] P. H. Lau, “Fire Resistance of Connections in Laminated Veneer Lumber (LVL),” University of Canterbury, 2006.

[35] Laplanche K, “Etude du comportement au feu des assemblages de structures bois: Approche expe´rimentale et mode´lisation,” Universite´ Blaise Pascal, 2006.

[36] Dhima D, “Verification experimentale de la resistance au feu des assemblages d’ e´le´ments en bois,” *CTICM Ref. INC-99/399-DD/NB*. CTICM, Paris, France, 1999.

[37] EN 1995-1-1, “Eurocode 5: design of timber structures—part 1-1: general—common rules and rules for buildings,” *CEN*. Brussels, 2006.

[38] NZS 3603:1993, “Timber structures standard,” *Standards New Zealand*. SNZ, Wellington, 1993.

[39] CAN/CSA-O86-09, “Engineering design in wood.” Canadian Standards Association, Rexdale, 2009.

[40] J. Noren, “Load-bearing Capacity of Nailed Joints Exposed to Fire,” *Fire Mater*, vol. 20, no. 3, pp. 133–143, May 1996, doi: 10.1002/(SICI)1099-1018(199605)20:3<133::AID-FAM565>3.0.CO;2-3.

[41] L. Peng, G. Hadjisophocleous, J. Mehaffey, and M. Mohammad, “Fire Performance of Timber Connections, Part 1: Fire Resistance Tests on Bolted Wood-Steel-Wood and Steel-Wood-Steel Connections,” *Journal of Structural Fire Engineering*, vol. 3, no. 2, pp. 107–132, Jun. 2012, doi: 10.1260/2040-2317.3.2.107.

[42] M. Gillet, L. Autrique, and L. Perez, “Mathematical model for intumescent coatings growth: application to fire retardant systems evaluation,” *J Phys D Appl Phys*, vol. 40, no. 3, pp. 883–899, Feb. 2007, doi: 10.1088/0022-3727/40/3/030.

[43] C. Di Blasi, “Modeling the effects of high radiative heat fluxes on intumescent material decomposition,” *J Anal Appl Pyrolysis*, vol. 71, no. 2, pp. 721–737, Jun. 2004, doi: 10.1016/j.jaap.2003.10.003.

[44] A. Öchsner, “Euler–Bernoulli Beam Theory,” *Classical Beam Theories of Structural Mechanics*. 2021.

[45] “European Standard, Eurocode 1: Actions on structures - Part 1-2: General actions - Actions on structures exposed to fire, vol. 1, no. 2. 2002.,” 1991.

[46] K. Livkiss, B. Andres, N. Johansson, and P. van Hees, “Uncertainties in modelling heat transfer in fire resistance tests: A case study of stone wool sandwich panels,” *Fire Mater*, vol. 41, no. 7, pp. 799–807, Nov. 2017, doi: 10.1002/fam.2419.

Appendix A

MATLAB code for the Image processing described in Section 2.2.1

Video to image sequence

```
movie = VideoReader('20mil-2.mp4')
n = movie.NumFrames;
       vidHeight = movie.Height;
       vidWidth = movie.Width;
    for i=1:30:n
        frames=read(movie,i);
        imwrite(frames,[int2str(round(i/30)), '.jpg']);
        im(i)=image(frames);
    end
```

Image processing

```
%reference measurement in pixel
distx=sqrt((448-16)^2 + (152-148)^2);
disty=sqrt((16-15)^2 + (244-148)^2);
%conversionunit mm/pixel
dx=24*25.4/distx;
dy=1*25.4/disty;
%origin top left
%corner points bottom left and top right in consideration
ybot=142;
ytop=60;
xleft=46;
xright=425;

measure=zeros(1,499);



for i=1:499
%     if i<30
%         ytop=55;
%     elseif i<51
%             ytop=40;
%     else
%         ytop=2;
%     end
%     % read image
C=imread(int2str(i),"jpg");
BW=imbinarize(C);
% figure
```

```
% imshowpair(C,BW,'montage')
I=zeros(ybot,xright+20,3);
I(ytop:ybot,xleft:xright,:)=BW(ytop:ybot,xleft:xright,:);
flag=0;
for y=ytop:ybot
    len=0;
    for x=xleft:xright
        if I(y,x,1)==1 && I(y,x,2)==0 && I(y,x,3)==0
            len=len+1;
        end
        if len>=20
            flag=1;
            break;
        end
    end
  if flag==1
      break;
  end
%  imshowpair(C,BW,'montage')
% yline(y,'g')
end
measure(i)=(142-y)*dy;
end
```

Commercial Intumescent coatings

Tested for fire resistance

Steel substrate

Firetex® FX5120
- 2hr fire protection IAW UL 263 (ASTM E-119)
- thin-film
- water-based

Albi Clad TF
- UL listed for 1 through 3-1/2hr to ASTM E-119
- thin film
- water-based

Thermo-Sorb® 263
- up to a 4hr fire rating
- tested IAW ASTM E-119 (UL 263)
- thin film
- solvent based

Wood substrate

FlameOFF® Fire Barrier Paint
- Tested and compliant with ASTM E119/UL 263
- 2 hr. fire protection (Non-load bearing)
- 1 hr. rating 30 mil DFT
- Primer - recommended but not required
- Available as 5-gallon pail
- Thin film
- Water-based
- Product may be applied by brush or spray application
- Application rate
    - Spray: 45 mils (1.14 mm) per coat (wet)
    - Brush: 10 mils (0.25 mm) per coat (wet)

Albi Clad FP
- Tested for 1 hr. fire resistance on wood, drywall and concrete
- ASTM E-119 / UL263
- Thin film
- Water-based
- Recommends use of airless spray equipment
    - For very small jobs, may be applied by trowel or palming method.
- Testing of ASTM E119 done at 40 mil thickness
- Available as 5-gallon pail

Tested for flammability

Wood

DC360

- Class A fire protection IAW ASTM E84
- used to reduce the flammability and smoke development
- water based intumescent coating
- materials such as OSB/Plywood, gypsum and lumber
- protect combustible substrates from fire for up to 30 minutes

WT-102

- White Flat Latex Intumescent Fireproofing Flame Retardant Paint Coating for Wood

FireGuard E-84 Intumescent Coating

- ASTM E-119, ASTM E-84 Tested
- Water-based
- Thin film

FSP FX-100

- ASTM E84 certified
- two-part system
- Class A or B protection

Commercial MgO coatings

MgO based fire retardant OSB
Constant MgO thickness so scaling possible only in OSB thickness

LP FLAMEBLOCK

- performance categories: 7/16″, 15/32″, and 19/32″

MagTech

- 1 1/8 and 15/32” thicknesses OSB

Charring in half-lap joints

Half-scale

Quarter-scale